

Geometry of Comparisons

Puoya Tabaghi

University of Illinois at Urbana-Champaign

Ivan Dokmanić

University of Basel

Abstract

Many data analysis problems can be cast as distance geometry problems in *space forms*—Euclidean, elliptic, or hyperbolic spaces. We ask: what can be said about the underlying space form if we are only given a subset of comparisons between pairwise distances, without computing an actual embedding? To study this question, we define the *ordinal capacity* of a metric space. Ordinal capacity measures how well a space can accommodate a given set of ordinal measurements. We prove that the ordinal capacity of a space form is related to its dimension and curvature sign, and provide a lower bound on the embedding dimension of non-metric graphs in terms of the *ordinal spread* of their sub-cliques. Finally, we show how the statistics of ordinal spread can be used to identify the underlying space form of similarity graphs on weighted trees and gene expression data.

1 INTRODUCTION

Distances reveal the geometry of their underlying space. Even distance *comparisons* carry valuable information. Let us consider a set of points x_1, \dots, x_N in space S . In non-metric embedding problems, we have measurements of the form

$$y_{i,j} = \phi(d(x_i, x_j)), i, j \in \{1, \dots, N\},$$

where $d(x_i, x_j)$ is the distance between x_i and x_j , and $\phi(\cdot)$ is an unknown monotonic increasing (or decreasing) function. We can only interpret these measurements as distance comparisons, or ordinal measurements, since

$$\phi(d(x_i, x_j)) \leq \phi(d(x_k, x_l)) \Leftrightarrow d(x_i, x_j) \leq d(x_k, x_l).$$

It is then natural to ask: *What do distance comparisons tell us about the space?*

Euclidean distance geometry problems (DGP) have a rich history in the literature from robotics [28, 34] and wireless sensor networks [32] to molecular conformations [7] and dimensionality reduction [25]. Typically, we want to find a representation for a set of measured Euclidean distances [10]. Beyond Euclidean DGPs, there has recently been a surge in applications of hyperbolic geometry in data analysis, most notably as a natural space to work with hierarchical data. Social networks [39], gene ontologies [2], and Hearst graph of hypernyms [23] are examples of hierarchical data. Similarly, spherical embedding aims to embed a set of objects on a (hyper)sphere given their dissimilarities [41] with various applications in astronomy [13], distance problems on Earth [3], and texture mapping [11]. *To compute an embedding, we have to know the geometry of embedding space.*

Euclidean, spherical and hyperbolic geometry are categorical examples of constant curvature spaces, known as space forms. A space form is characterized by its curvature and dimension. For non-metric embedding problems posed in space forms, we want to characterize these two properties from the measured distance comparisons. However, it is impossible to infer the magnitude of a space form’s curvature only based on distance comparisons. In other words, if a set of distance comparisons is realizable in a space form with curvature 1 (or -1), then we can find an equivalent embedding in a space form with curvature C (or $-C$) for any positive C . *In this paper, we show that ordinal measurements carry information about the curvature sign and dimension of space forms.*

1.1 Motivation and Related Work

In many applications, we want to find a representation for a group of entities based on their distances, but the exact magnitude of distances might be unavailable. This is prevalent in applied research fields like neural coding [12], developmental biology [21], learning from perceptual data [9], and cognitive psychology [26].

Non-metric embedding problems date back to the works of Shepard [30, 31] and Kruskal [22]. Inspired by the Shepard-Kruskal scaling problem, Agarwal *et al.* pro-

pose generalized non-metric multidimensional scaling, a semidefinite relaxation to embed dissimilarity (or similarity) ratings of a set of entities in Euclidean space [1]. Stochastic triplet embedding [38] and crowd kernel learning [35] aim to embed probabilistic notions of triadic comparisons. Tabaghi *et al.* propose a semidefinite relaxation for metric and non-metric embedding problems in hyperbolic space [33].

The embedding space should properly represent the measured data. For example: In developmental biology, single cell RNA sequencing (scRNAseq) are used to propose data-driven definitions of cell identity and function. This has important implications for clustering, lineage identification, and studying dynamic cellular processes [36]. Recently, Klimovskaia *et al.* proposed to use hyperbolic spaces to better represent the hierarchical structure of single-cell measurements, compared to conventional Euclidean spaces [21]. It is therefore necessary to first identify the underlying space, before the actual embedding. In Section 5.2, we consider discovering information about the embedding space in the setting of non-metric embedding of scRNAseq data.

Learning from distance comparisons is an active area of research. Among relevant research topics are ranking objects from pairwise comparisons [40, 18], theoretical analysis of necessary number of distance comparisons to uniquely determine the embedding [19], nearest neighbor search [14], random forests [15], and classification based on triplet comparisons [8]. Understanding the underlying geometry of ordinal measurements is important in designing relevant algorithms.

Related to non-metric embedding problems are the various topological techniques. They study geometric properties of point clouds by ignoring the actual choice of metrics and sensitive geometric properties such as curvature [4]. A related problem is to detect intrinsic structure in neural activity, invariant under nonlinear monotone transformations of measurements. Giusti *et al.* [12] propose a method based on clique topology of the graph of correlations between pairs of neurons. Clique topology of a weighted graph describes the behavior of cycles in its order complex¹ as a function of edge densities, also known as *Betti curves*. The statistical behavior of Betti curves can help distinguish random and geometric structures of size $N \approx 100$ in Euclidean space. Zhou *et al.* [43] generalize this statistical approach to hyperbolic spaces.

¹Order complex of a complete, weighted graph K_N is a sequence of graphs $G_0, \dots, G_{\binom{N}{2}}$ where G_0 is the graph having N vertices and no edges, G_1 has a single edge corresponding to the highest edge weight of G , and each subsequent graph has an additional edge for the next-highest edge weight [12].

Main contributions: We propose a framework to study the geometry of distance comparisons based on (1) appearance pattern of vertices in sorted distance lists, and (2) ordinal capacity of underlying space form.

Ordinal capacity of a metric space (S, d) is the maximum number of points $x_1, \dots, x_N \in S$ such that

$$\sup_{n \in [N-1]} d(x_n, x_N) \leq \inf_{\substack{i, j \in [N-1] \\ i \neq j}} d(x_i, x_j)$$

where $[N-1] = \{1, \dots, N-1\}$.

Ordinal capacity of a metric space characterizes the admissible patterns of ordinal measurements. For instance, in a Euclidean space with fixed dimension d , we claim that only specific patterns of distance comparisons, e.g.,

$$d(x_i, x_j) \leq d(x_k, x_l), \quad i, j, k, l \in [N]$$

are realizable. We show that the ordinal capacity of a space form is only related to its dimension and curvature sign. On the other hand, we define the *ordinal spread* for a point set to describe their appearance pattern in the sorted distance list. The theoretical relation between ordinal capacity and ordinal spread gives us a distribution-free lower bound for Euclidean and spherical embedding dimensions of non-metric data.

Finally, we associate ordinal spread variables with the ordinal measurements and compare their statistical properties to typical variables from each space form. This serves as a practical tool to identify the underlying space form of large similarity graphs. In Section 5, we show that this analysis can correctly uncover the hyperbolicity of weighted trees, and identify the proper space form for ordinal measurements related to scRNAseq data. All proofs, algorithms, and further discussions are available in Supplementary Materials.

2 NON-METRIC DISTANCE PROBLEMS IN SPACE FORMS

A space form is a complete, connected Riemannian manifold of dimension $d \geq 2$ and constant sectional curvature. Space forms are equivalent to spherical, Euclidean, or hyperbolic spaces up to an isomorphism [24]; see Table 1.

Distance geometry problems aim to find an embedding for a set of distance-related measurements in a metric space. They can be metric [33], non-metric [1], or unlabeled [17] depending on the data modality and application domain. In this paper, we focus on non-metric distance problems in space forms.

Table 1: Space forms, their metric, and sectional curvature $K_x(\sigma)$ of a tangent subspace σ at x .

	Hyperbolic (Poincaré Model)	Euclidean	Hyperspherical
S	$\mathbb{H}_C^d = \{x \in \mathbb{R}^{d+1} : \langle x, x \rangle = C^{-1}\}$	\mathbb{E}^d	$\mathbb{S}_C^d = \{x \in \mathbb{R}^{d+1} : \langle x, x \rangle = C^{-1}\}$
$d(x, y)$	$ C ^{-\frac{1}{2}} \operatorname{acosh}(C[x, y])$	$\sqrt{\langle x - y, x - y \rangle}$	$C^{-\frac{1}{2}} \operatorname{acos}(C\langle x, y \rangle)$
$K_x(\sigma)$	$C < 0$	0	$C > 0$

Problem 1. Let S be a space form with distance function $d : S \times S \rightarrow \mathbb{R}^+$. A non-metric space form distance geometry problem aims to find $x_1, \dots, x_N \in S$, given a subset of ordinal distances measurements \mathcal{O} such that

$$d(x_{i_1}, x_{i_2}) \leq d(x_{i_3}, x_{i_4}), \quad \text{for all } i \in \mathcal{O} \subseteq [N]^4 \quad (1)$$

where $i = (i_1, i_2, i_3, i_4)$.

Kleindessner *et al.* study the uniqueness of such embedding functions in Euclidean spaces, up to an isotony [20]. For noise-free measurements, we can fully encode distance comparisons in a sorted list, namely

$$d(x_{i_1}, x_{j_1}) \geq \dots \geq d(x_{i_{\binom{N}{2}}}, x_{j_{\binom{N}{2}}}). \quad (2)$$

We assume that such a list always exists and is unique. A deterministic or a randomized binary sort algorithm needs at least $\Theta(\binom{N}{2} \log \binom{N}{2})$ pairwise comparisons to uniquely sort the distance list [6].

Example 1. Consider a set of points $x_1, \dots, x_6 \in \mathbb{R}^2$ that form a centered, regular pentagon shown in Figure 2 (a). A sorted distance list could be

$$d(x_2, x_4) \geq d(x_2, x_5) \geq d(x_3, x_1) \geq \dots \geq d(x_6, x_5).$$

We summarize the indices appearing in the sorted distance list in the index matrix Λ ,

$$\Lambda = \begin{bmatrix} 2 & 2 & 3 & \cdots & 6 \\ 4 & 5 & 1 & \cdots & 5 \end{bmatrix} \quad (3)$$

where the k -th column represents the index pairs appearing at the k -th position in the sorted distance list.

Alternatively, we can represent this sequence in a $N \times \binom{N}{2}$ binary index matrix $M = (m_{ij})$. If x_i appears in the j -th position of the distance list (2), then $m_{ij} = 1$. Otherwise, $m_{ij} = 0$; see Figure 1. In the next section, we use the index matrix to extract useful information about the geometry of underlying space.

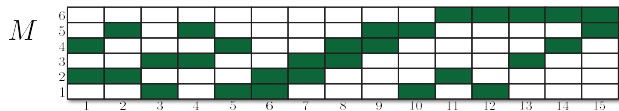


Figure 1: Rows of the binary index matrix M correspond to point indices that appear in distance list of Example 1.

3 ORDINAL SPREAD

We consider identifying space form S from a given set of distance comparisons in Problem 1. In Section 2, we showed how this problem is equivalent to inferring geometrical information through the (sorted) distance list associated with the pairwise comparisons. Any geometry-related inference must be invariant with respect to arbitrary permutations of point indices. It will be useful to devise a canonical procedure to relabel each point. We uniquely relabel each point in accordance to the position of its first appearance in the distance list.

Example 2. Consider the points in Figure 2 (a) with the index matrix Λ given in (3). The following sequence shows their appearance order in the distance list,

$$x_2 \rightarrow x_4 \rightarrow x_5 \rightarrow x_3 \rightarrow x_1 \rightarrow x_6.$$

The canonical ordering of the labels assigns $x_{(1)}$ and $x_{(2)}$ to the largest distance, $x_{(3)}$ to the second largest distance, etc., and produces the following sequence

$$x_{(1)} \rightarrow x_{(2)} \rightarrow x_{(3)} \rightarrow x_{(4)} \rightarrow x_{(5)} \rightarrow x_{(6)}.$$

As a result, this process permutes the rows of the binary index matrix M .

The appearance pattern of *new* points in the distance list is *invariant* to point labels and bears geometrical implications. We formalize this notion in Definition 1.

Definition 1. The k -th ordinal spread of the point set $X = \{x_n\}_{n=1}^N$ is defined as

$$\alpha_k(X) = \min_{1 \leq m \leq \binom{N}{2}} \left\{ \operatorname{card} \bigcup_{s=1}^m \{ \lambda_{1,s}, \lambda_{2,s} \geq k \} \right\}.$$

$\Lambda = (\lambda_{i,m})_{i \in [2], m \in \binom{N}{2}}$ is the index matrix. We simply write α_k where no confusion can arise.

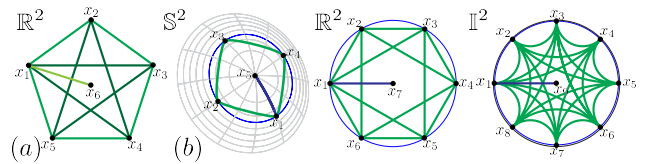


Figure 2: (a): An example of a point configuration in \mathbb{R}^2 . (b): Point sets in spherical (\mathbb{S}^2), Euclidean (\mathbb{R}^2) and hyperbolic (Poincaré disk \mathbb{I}^2) spaces with maximum (N -th) ordinal spread.

The k -th ordinal spread of a point set is the position of the first appearance of $x_{(k)}$ in the sorted distance list. In other words, we have

$$\text{card} \bigcup_{m=1}^{\alpha_k-1} \{\lambda_{1,m}, \lambda_{2,m}\} < k, \text{ card} \bigcup_{m=1}^{\alpha_k} \{\lambda_{1,m}, \lambda_{2,m}\} \geq k.$$

Example 3. For the point set shown in Figure 2 (a) with index matrix (3), we have

$$\begin{aligned} \alpha &= (\alpha_1, \alpha_2, \alpha_3, \alpha_4, \alpha_5, \alpha_6) \\ &= (1, 1, 2, 3, 3, 11). \end{aligned}$$

Fact 1. Let $\{x_n\}_{n=1}^N$ be a set of points in (S, d) . The ordinal spread vector is invariant with respect to strongly isotonic transformation [20] of points. In other words, let $\psi : S \rightarrow S$ be an arbitrary function such that for all $x, y, z, w \in S$ we have

$$\begin{aligned} d(x, y) < d(z, w) &\Rightarrow d(\psi(x), \psi(y)) < d(\psi(z), \psi(w)), \\ d(x, y) = d(z, w) &\Rightarrow d(\psi(x), \psi(y)) = d(\psi(z), \psi(w)), \end{aligned}$$

$$\text{then, } \alpha(\{x_n\}_{n=1}^N) = \alpha(\{\psi(x_n)\}_{n=1}^N).$$

Proposition 1. For any point set $X = \{x_n\}_{n \in [N]}$ in a metric space, we have

- $\alpha_1(X) = \alpha_2(X) = 1, \alpha_3(X) = 2,$
- $\lceil \frac{N}{2} \rceil \leq \alpha_N(X) \leq \binom{N-1}{2} + 1.$

Let us devise an experiment to show how the k -th ordinal spread can distinguish space forms. We randomly generate i.i.d. points $\{x_n\}_{n=1}^N$ from absolutely continuous distributions with full support in hyperbolic, Euclidean and spherical spaces.² In Figure 3, we plot the k -th ordinal spread α_k for each realization $\{x_n\}_{n=1}^N$. We find the empirical maximum of α_N to be the most sensitive indicator of the geometry of underlying space. While the emerging pattern of α_N 's is dependent on the distribution of point sets, the behavior of empirical maximum of N -th ordinal spread is robust to the choice of point set distributions, as it converges to its supremum almost surely. Therefore, we introduce the N -point ordinal spread for a metric space – a tool to categorize space forms based on their ability to house extremal ordinal patterns, in the sense of Definition 2.

Definition 2. Let S be a metric space. The N -point ordinal spread of S is defined as

$$A_N(S) = \sup_{x_1, \dots, x_N \in S} \alpha_N(\{x_n\}_{n=1}^N).$$

²Uniform distribution for spherical, and projected normal for hyperbolic space, i.e., $y = [\sqrt{1 + \|x\|^2}, x^\top]^\top$ where $x \sim \mathcal{N}(0, I)$.

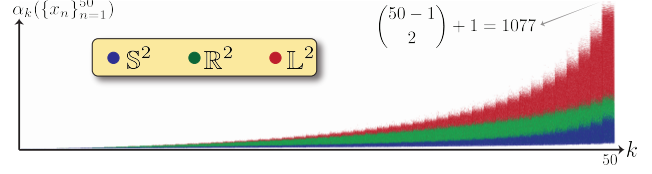


Figure 3: The k -th ordinal spread of 10^5 randomly generated points $\{x_n\}_{n=1}^{50}$ in 2-dimensional space forms.

The ordinal spread number of a space form depends on extremal configurations of point sets. In Figure 2 (b), we show point sets with maximum $(N$ -th) ordinal spread α_N of $\binom{N-1}{2} + 1$; see Proposition 1. In the next section, we introduce *ordinally dense subsets*, and show how they determine the N -point ordinal spread of space forms.

4 ORDINAL CAPACITY

Definition 3. Let x_1, \dots, x_N be a set of distinct points in metric space S . If

$$\sup_{n \in [N-1]} d(x_n, x_N) \leq \inf_{\substack{i, j \in [N-1] \\ i \neq j}} d(x_i, x_j),$$

then we say that $\{x_n\}_{n=1}^N$ is an *ordinally dense subset* of S , or in short $\{x_n\}_{n=1}^N \subseteq S$.

Definition 3 formalizes the point configurations with maximum ordinal spread. A set of N points is *ordinally dense* in S if and only if it has a subset of $N-1$ points whose pairwise distances are **all** larger than (or equal to) their distances to the N -th point, i.e.,

$$\{x_n\}_{n=1}^N \subseteq S \iff \alpha_N(\{x_n\}_{n=1}^N) = \binom{N-1}{2} + 1.$$

The existence of an *ordinally dense* subset of size N depends on the curvature sign and dimension of space forms. Henceforth, we want to find the maximum number of *ordinally dense* points in space forms.

Definition 4. The *ordinal capacity* for a metric space S is defined as

$$K(S) = \sup \{ \text{card} \{x_n\} : \{x_n\} \subseteq S \}.$$

The ordinal capacity is an indicator of the capability of a metric space to accommodate different patterns of point labels. For space forms, this concept is intimately related to the famous spherical cap packing problem [29], as the proof of the following theorem shows.

Theorem 1. The ordinal capacity for a space form S is given by

$$K(S) = \begin{cases} +\infty, & \text{if } S \cong \mathbb{H}^d \\ \leq \rho_d + 1, & \text{if } S \cong \mathbb{E}^d, S \cong \mathbb{S}^d \end{cases}$$

$$\text{where } \rho_d = \left\lfloor \sqrt{\frac{\pi}{2}} \frac{\Gamma(\frac{d-1}{2})}{\Gamma(\frac{d}{2}) \int_0^{\frac{\pi}{4}} \sin^{d-2} \theta \left(\cos \theta - \frac{\sqrt{2}}{2} \right) d\theta} \right\rfloor = O(2^{\frac{d+3 \log_2 d}{2}}).$$

Table 2: Numerical values for ρ_d .

d	1	2	3	4	5	6	7	8	9
ρ_d	2	6	15	31	59	106	183	308	507

The ordinal capacity of a hyperbolic space is infinite. This implies that there exists an ordinally dense point set $\{x_n\}_{n=1}^N$ for any $N \in \mathbb{N}$. In Poincaré model, a centered regular $(N-1)$ -gon with an extra point in the center is an ordinally dense set; see Figure 2 (b). In comparison, Euclidean and spherical spaces have finite ordinal capacities, increasing exponentially³ with their dimensions as given in Table 2.

Example 4. In Figure 2 (b), all distances in the hexagon are larger or equal to their distances to the center. In fact, this point set realizes $K(\mathbb{R}^2) = 7$.

The ordinal capacity can not be used to distinguish between \mathbb{S}^d and \mathbb{R}^d . This is intuitive since an arbitrary small open neighborhood in a d -sphere has the same ordinal capacity as a d -dimensional Euclidean space. However, it is possible to refine the ordinal capacity of spherical space if we only consider points set $\{x_n\}$ with a minimum distance constraint; see Supplementary Materials.

In Theorem 2, we show the direct relation between ordinal capacity and ordinal spread of a space form.

Theorem 2. The N -point ordinal spread of a space form S is given by

$$A_N(S) = E(T(N-1, K(S)-1)) + 1$$

where $E(T(N, K))$ is the number of edges of $T(N, K)$, the K -partite Turán graph [37] with N vertices.

4.1 Visualizing Ordinal Capacity

Let us devise a numerical experiment to get a geometrical intuition about the notion of ordinal capacity. We generate i.i.d. point sets $\{x_n\}_{n=1}^N$ from a (projected) normal distribution in 2-dimensional hyperbolic and Euclidean spaces. For each trial, we plot the ordinal spread $\alpha_N(\{x_n\}_{n=1}^N)$ of each realization and for varying sizes of point sets N . The maximum ordinal spread of the generated point sets gives an estimate for the N -point ordinal spread of Euclidean and hyperbolic spaces; see Definition 2. We repeat this experiment by fixing a point at the center of the coordinate system, and projecting the remaining points to their circumscribed circle, i.e., the point sets $\{y_n\}_{n=1}^N$ where

$$y_N = 0 \text{ and } y_n = r^{-1}x_n \quad \forall n \in [N-1],$$

where $r = \max_{n \in [N-1]} \|x_n\| + \epsilon$, for a small $\epsilon > 0$.

³Their ordinal capacities have a lower bound of the form $\exp(d \log 2 + o(d))$ [42]; see Supplementary Materials.

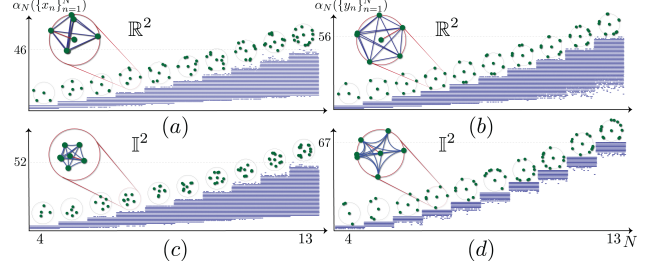


Figure 4: Ordinal spread of 5×10^5 i.i.d. point sets in \mathbb{R}^2 and \mathbb{I}^2 , in top and bottom rows. For a fixed N , we show the point set with the maximum ordinal spread – $\{x_n\}_{n=1}^N$ for Figures (a, b) and $\{y_n\}_{n=1}^N$ for Figures (b, d). The partitions in Figures (b, d) resemble the ordinally dense point sets shown in Figure 2 (b).

The random points $\{y_n\}_{n=1}^N$ yield a more accurate estimate for the $A_N(\mathbb{I}^2)$ and $A_N(\mathbb{R}^2)$; see Figure 4. We also show individual points in sets with maximum ordinal spread accumulate on non-overlapping spherical caps of the circle; see the proof of Theorems 1 and 2. For example, we show that there are 5 strictly non-overlapping spherical caps for 2-dimensional Euclidean space, whereas this number is infinite for hyperbolic spaces. Therefore, ordinal capacity of a space form equals the total number such caps plus the center point.

The distribution of data points determines the statistical properties of their ordinal spread. Nevertheless, the estimated N -point ordinal spread of Euclidean space is close to the theoretical bound, e.g., we have $\hat{A}_{13}(\mathbb{R}^2) = 56$, whereas the theoretical bound is $A_{13}(\mathbb{R}^2) \leq 58$. The estimated N -point ordinal spread of a hyperbolic space matches its theoretical bound of $A_N(\mathbb{I}^2) = \binom{N-1}{2} + 1$.

4.2 Distribution-Free Lower Bound for Embedding Dimension

In non-metric embedding applications, we are given a set of entities and their pairwise dissimilarities $\{y_{i,j}\}_{i,j \in [N]}$. Therefore, we may assume that similarity measurements are related to embedded points $\{x_n\}_{n \in [N]}$ through a monotonically increasing function ϕ ,

$$y_{i,j} = \phi(d(x_i, x_j)), \quad \forall i, j \in [N].$$

A similar model can be proposed for similarity measurements. The main assumption is the existence of such a point set,

$$\exists x_1, \dots, x_N \in S : d(x_i, x_j) = \phi^{-1}(y_{i,j}), \quad \forall i, j \in [N]$$

where (S, d) is the target metric space, and ϕ is any monotonically increasing function.

Given similarity measurements of M entities, we can compute the ordered distance list, ordered index matrix,

and ordinal spread of sub-cliques in the presumed point set $X \subseteq \{x_m\}_{m=1}^M$ where $\text{card } X = N \ll M$. On the other hand, Theorem 2 gives a universal upper bound for ordinal spread of point sets in space forms. Hence, we can use it to find a bound on minimum dimension \hat{d} for a space form that can accommodate this set of ordinal measurements.

In practice, we calculate the empirical N -th ordinal spread for a set of non-metric measurements associated with the point set $\{x_n\}_{n=1}^N$, i.e.,

$$\hat{A}_N = \sup_{\substack{X \subseteq \{x_m\}_{m \in [M]}, \\ \text{card } X = N}} \alpha_N(X),$$

where $N \ll M$. Then, we can find a lower bound for Euclidean (or spherical) embedding dimension \hat{d} by computing

$$\hat{d} = \max_{N \in [M]} \arg \min_d \left(\hat{A}_N \leq A_N(\mathbb{R}^d) \right). \quad (4)$$

The main remarks regarding this approach are:

- Equation (4) gives a universal lower bound for Euclidean/spherical embedding dimension, and is invariant to underlying distribution of point sets.
- The ordinal spread of space forms — the upper bound in (4) — depends on the extreme configurations of point sets with maximum spread, e.g., point sets in Figure 2 (b). In applications, the data points (or more precisely, the measured dissimilarities) rarely have large sub-cliques with maximum ordinal spread. Therefore, the lower bound in (4) is a conservative estimate of the embedding dimension.
- We can not apply this test to estimate the dimension of hyperbolic spaces since they have infinite ordinal capacities, regardless of their dimension. Therefore, for any measurements in a d -dimensional hyperbolic space, we get the trivial lower bound of $\hat{d} = 2$.

4.3 Statistical Tests for Space Forms' Curvature and Dimension

We can devise a more powerful test if we have access, via an oracle, to the distribution of embedded points. Let $x_1, \dots, x_N \in S$ be i.i.d. random points drawn from probability distribution P_x^S . Therefore, the k -th ordinal spread is a random variable, i.e.,

$$\alpha_{k,N} \stackrel{\text{def}}{=} \alpha_k(\{x_n\}_{n \in [N]}), \quad x_n \sim P_x^S, \quad \forall n \in [N].$$

The distribution of $\alpha_{k,N}$ is invariant with respect to strongly isotonic transformation of underlying points. Also, regardless of distribution P_x^S , the N -th ordinal spread of space forms determines the support of ordinal spread variables $\alpha_{k,N}$. Specifically, we have

$$\alpha_{k,N} \leq A_k(S), \text{ almost surely.}$$

Now, let us assume that an oracle gives us the distribution of embedded N points in a space form S . Accordingly, we can calculate the distribution of the k -th ordinal spread, $P_{\alpha_{k,N}}^S$, or even the joint distribution of ordinal spread vector, $P_{\alpha_N}^S$, at least in principle.

Thus, we propose a hypothesis test based on the distance between a set of distributions picked by the oracle and the empirical distribution derived from ordinal measurements. Given similarity measurements for a number of M entities, the empirical probability mass function (pmf) of $\alpha_{k,N}$, for $N \ll M$, can be estimated from

$$\hat{P}_{\alpha_{k,N}}(r) = \left[\binom{M}{N} \right]^{-1} \sum_{\substack{X \subseteq \{x_m\}_{m \in [M]}, \\ \text{card } X = N}} [\alpha_k(X) = r],$$

where the Iverson bracket $[P] = 1$ if P is true and is 0 otherwise. The empirical pmf $\hat{P}_{\alpha_{k,N}}$ is a U -statistic of order M with the kernel $[\alpha_k(X) = r]$ [16]. This is an unbiased estimator with $\text{Var} \left\{ \hat{P}_{\alpha_{k,N}}(r) \right\} = O\left(\frac{N^2}{M}\right)$ for large M .

We define the *best* embedding space form S^* to have the minimum divergence between empirical and oracle distributions of ordinal spreads. For example, the space form that best matches the empirical distribution of $\alpha_{k,N}$ is given by

$$S^* = \arg \min_{S \in \{S_1, \dots, S_K\}} \delta(P_{\alpha_{k,N}}^S, \hat{P}_{\alpha_{k,N}}),$$

where S_1, \dots, S_K is a collection of space forms, and $\delta(\cdot, \cdot)$ is a suitable metric on the space of probability measures, e.g., total variation distance.

In many applications, unfortunately, we do not have access to oracle distribution P_x^S , or equivalently $P_{\alpha_{k,N}}^S$. In Section 5, we show how to use *side information* to infer some necessary properties for the distribution of data points P_x^S . This approach correctly reveals the negative curvature of embedding space for weighted trees, and appropriate spaces for comparison measurements derived from scRNAseq data.

5 NUMERICAL EXPERIMENTS

5.1 Distance Comparisons Reveal Hyperbolicity of Trees

Hyperbolic spaces are ideal space forms for embedding trees. In this section, we design experiments to confirm the hyperbolicity of metric (weighted) graphs only from distance comparisons.

This analysis is based on the statistical behavior of the extracted ordinal spread variables $\alpha_{k,N}$. We generate a

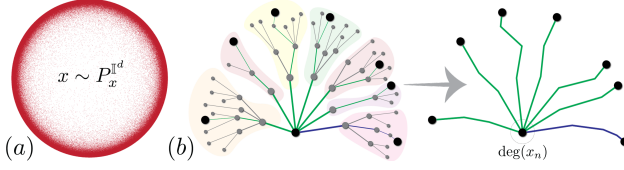


Figure 5: (a) : Random samples from projected normal distribution $P_x^{\mathbb{I}^2}$; (b) : The selected point set (of size $\deg(x_n) + 1$) has the maximum ordinal spread.

random tree T with $N = 10^4$ nodes, maximum degree of Δ , and i.i.d. edge weights from $\text{unif}(0, 1)$. Let $\tilde{D}_\Delta = D_\Delta + n$ be the noisy distance matrix for T , where the distance between each two nodes is defined as the weight of the path joining them. The embedding goal is to find a representation x_1, \dots, x_N for tree nodes in S , such that

$$d(x_i, x_j) \leq d(x_k, x_l) \iff \tilde{D}_\Delta(i, j) \leq \tilde{D}_\Delta(k, l).$$

We randomly select 10^6 sub-cliques of sizes $N \in \{2, 4, \dots, 20, 100\}$. In Table 3, we give the empirical N -th ordinal spread based on non-metric measurements associated with the sub-cliques, i.e., \hat{A}_N . The distribution-free test (4) gives a lower bound of $\hat{d} \geq 4$ for Euclidean embedding dimension.

On the other hand, consider a random weighted tree and a node x_n with degree Δ_n .⁴ We can easily see that

$$\max_{i \in [\Delta_n]} d(x_n, x_{n_i}) \leq \min_{\substack{i, j \in [\Delta_n] \\ i \neq j}} d(x_{n_i}, x_{n_j}),$$

where $x_{n_1}, \dots, x_{n_{\Delta_n}}$ are adjacent points to x_n . Hence, $\{x_n\} \cup \{x_{n_i}\}_{i=1}^{\Delta_n}$ is a set of $\Delta_n + 1$ points with maximum ordinal spread; see Figure 5 (b). Therefore, a lower bound for embedding dimension of a metric tree T (in Euclidean space) is given by

$$\begin{aligned} \hat{d} &\geq \min \{d : K(\mathbb{R}^d) \geq \Delta(T) + 1\} \\ &= \min \{d : \rho_d \geq \Delta(T)\} \end{aligned}$$

The exponential growth of ρ_d gives $\hat{d} = \Omega(\log \Delta(T))$.

Following the statistical approach in Section 4.3, we assume the *oracle* picks a set of distributions for embedded points in each space form, viz. projected normal for

Table 3: The N -point ordinal spread for $\mathbb{R}^2, \mathbb{R}^3, \mathbb{R}^4$ versus \hat{A}_N estimated from \tilde{D}_3, \tilde{D}_4 and \tilde{D}_5 .

N	6	8	10	12	14	16	18	20	100
$\tilde{D}_3 : \hat{A}_N$	11	22	37	56	79	106	137	169	4421
$\tilde{D}_4 : \hat{A}_N$	11	22	37	56	79	106	136	172	4412
$\tilde{D}_5 : \hat{A}_N$	11	22	37	56	79	106	137	170	4454
$A_M(\mathbb{R}^2)$	11	21	34	51	71	94	121	151	4048
$A_N(\mathbb{R}^3)$	11	22	37	56	79	106	135	168	4573
$A_N(\mathbb{R}^4)$	11	22	37	56	79	106	137	172	4741

⁴We assume the existence of a perfect embedding.

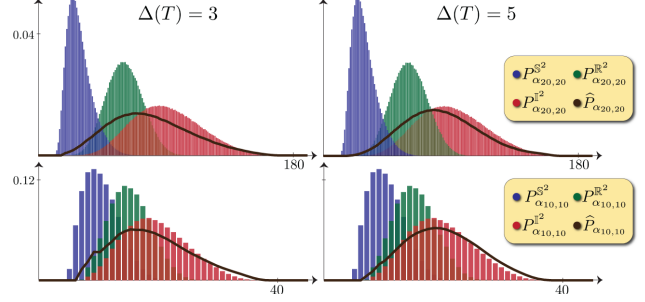


Figure 6: The empirical distributions of $\alpha_{20,20}$ and $\alpha_{10,10}$ for the trees with $\Delta(T) = 3, 5$.

hyperbolic and uniform distribution for Euclidean and spherical space; see Figure 5 (a). For each random tree, we construct the empirical pmf of $\alpha_{N,N}$, $N = 10, 20$. Then, we generate random points in S and estimate $P_{\alpha_{N,N}}^S$ for $S = \mathbb{S}^2, \mathbb{R}^2$ and \mathbb{I}^2 ; see Figure 6. Across different ordinal spread variables, hyperbolic spaces give better matches for the empirical distributions. For a detailed analysis on embedding dimensions and choices of point distributions refer to Supplementary Materials.

5.2 Single-cell Transcriptomic Data

RNA sequencing data capture the transcriptomes of cells, and are used to study the cell composition and developmental stages of organs. As Tanay *et al.* discuss, computational algorithms for clustering, detecting lineage, or inferring a pseudotemporal ordering of cells are based on *comparison* of transcriptomic profiles [27]. However, the comparison criterion has geometric implications for gene expression data. For instance, Klimovskaia *et al.* construct similarity probabilities from the relative forest accessibility (RFA) matrix [5], and claim that hyperbolic geometry is the ideal embedding space form [21].

We consider three experiments in which pairwise comparisons are made with respect to (1) angles, (2) Euclidean distances, and (3) RFA index for the digital gene expression matrix of adult planarians [27]. Let $x_1, \dots, x_N \in \mathbb{R}^d$ be cell expression vectors, where $N = 2.6 \times 10^4$ and $d = 2.1 \times 10^4$. We define the angle between two cells x_i, x_j as

$$\angle(x_i, x_j) \stackrel{\text{def}}{=} \arccos \frac{(x_i - \mu)^\top (x_j - \mu)}{\|x_i - \mu\| \|x_j - \mu\|}$$

where $\mu = \frac{1}{N} \sum_{n \in [N]} x_n$, and we denote their ℓ_2 distance as $\|x_i - x_j\|$. We construct the local connectivity edge set E from a symmetric k -nearest neighbor method on the points. RFA matrix is a $N \times N$ doubly stochastic matrix defined as $P = (I + L)^{-1}$ where $L = D - A$ is the Laplacian matrix, $A = (A_{i,j})$ such that

$$A_{i,j} = \exp \left(- \frac{\|x_i - x_j\|^2}{2\sigma^2} \right) [(i, j) \in E],$$

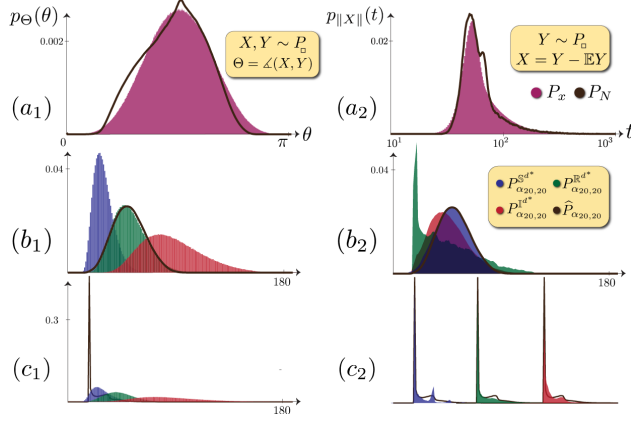


Figure 7: (a_1) : P_Θ for a normal distribution P_x ; (a_2) : $P_{\|Y - \mathbb{E}Y\|}$ for a log-normal distribution P_x . (b_1, b_2) and (c_1, c_2) : The empirical distribution of $\alpha_{20,20}$ for angle and ℓ_2 comparisons based on random points from normal and log-normal distributions, (b_1, c_1) and (b_2, c_2) .

and D is a diagonal matrix with $D_{ii} = \sum_{j \in [N]} A_{i,j}$. The ij -th element of P is the probability of a spanning forest includes a rooted tree at x_i and is connected to x_j — a measure of similarity between x_i and x_j [21].

Our goal is to identify high-dimensional spherical and Euclidean geometries for comparisons data derived from angles and ℓ_2 distances, and conjecture about the geometry of RFA comparisons. In this application, we have access to *side information* like the empirical distribution of pairwise angles and norms of centered points; see Figure 7 (a_1, a_2) .

The distribution of angles hints to an almost circularly symmetric point distribution such as (projected) Gaussian and uniform distributions on (hyperbolic) Euclidean and spherical spaces. With these prior distributions, this test incorrectly detect Euclidean space for angle comparisons, and fails to explain the spike in ordinal spread of ℓ_2 comparisons; see Figure 7 (b_1, c_1) . On the other hand, the empirical distribution of (centered) point norms hints to a heavy tailed distribution, e.g., log-normal distribution. Heavy tailed distributions frequently generate a distance list like $d(x_1, x_2) \geq d(x_1, x_3) \geq \dots \geq d(x_1, x_N)$, and cause a spike at $\alpha_{N,N} = N - 1$. Therefore, we use

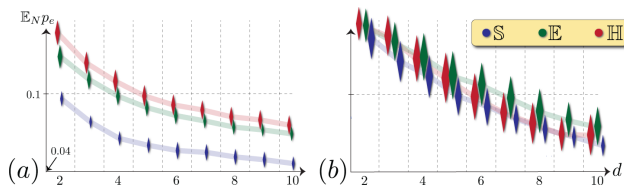


Figure 8: Empirical probability of incorrect comparisons and its standard deviation for embedded points in \mathbb{S}^d , \mathbb{E}^d and \mathbb{H}^d from (1) angle θ and (2) ℓ_2 norm comparisons.

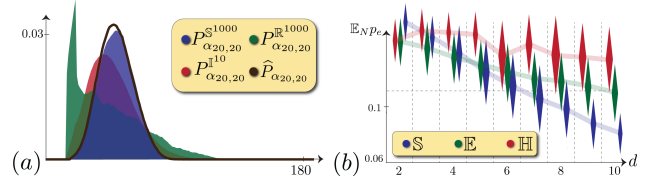


Figure 9: (a) : The statistical test for space forms with optimal dimensions and log-normal distribution P_x^{S*} . (b) : $\mathbb{E}_N p_e$ for embedded points from RFA comparisons.

log-normal point distribution and correctly identify the type of space forms; see Figure 7 (b_2, c_2) and Supplementary Materials for additional details. We repeat this test on RFA comparisons and with log-normal prior distribution for data points. We iterate over (1) various dimensions of each space form, and (2) parameters of log-normal distributions to find the optimal ordinal spread distributions in each Euclidean, spherical and hyperbolic spaces. We conjecture that the underlying geometry of RFA-based comparisons is a high (~ 1000) dimensional spherical space; see Figure 16.

Space form embedding algorithms aim to find a low-dimensional representation for a sequence of ordinal measurements that best preserves the pairwise comparisons [33, 1]. In graph-related applications, we want to have $d(x_i, x_j) \leq d(x_k, x_l)$ if nodes i, j are more similar compared to nodes k, l . For the gene expression data set, we report the empirical probability of incorrect comparison $\mathbb{E}_N p_e$ for different space forms of varying dimensions; see Figure 8, Figure 16 (b) , and Supplementary Materials for the detail of embedding methods. These results do not contradict our statistical analysis. However, the embedding quality, i.e., $\mathbb{E}_N p_e$, depends on how well the *ambient* space can be represented by a low-dimensional space. In comparison, our proposed analysis can only identify the *ambient* geometry of ordinal data — regardless of its dimension. Therefore, in order to study the low-dimensional embedding quality of non-metric data, we need further analysis on how well the data space can be approximated with a lower dimensional space form.

6 CONCLUSION

This paper offers a discussion about inferring the geometry of space forms from similarity comparisons between a set of entities. We introduce novel notions such as ordinal capacity and spread for metric spaces, as well as ordinally dense discrete sets. We provide theoretical and statistical analysis of ordinal spread variables. The proposed analysis, along with reasonable priors for the distribution of entities in a set of target spaces, can be used to identify the curvature sign of similarity graphs. This geometry driven approach for studying embedding spaces brings new perspective in designing algorithms related to similarity measurements.

Geometry of Comparisons: Supplementary Materials

7 PROOFS OF THEOREMS AND PROPOSITIONS

Notation For any two numbers $a, b \in \mathbb{R}$, we let $a \vee b$ and $a \wedge b$ be their maximum and minimum. We use small letters for vectors, $x \in \mathbb{R}^m$, and capital letters for matrices, $X = (x_{i,j}) \in \mathbb{R}^{m \times n}$. We denote the m -th standard basis vector in \mathbb{R}^M by e_m , $m \in [M]$ and let $[M]$ be short for the set $\{1, \dots, M\}$. For vectors $x, y \in \mathbb{R}^{d+1}$, their dot product is denoted by $\langle x, y \rangle$, and their Lorentzian inner product is $[x, y] = -x_0 y_0 + \sum_{i=1}^d x_i y_i$. The d -dimensional Poincaré model of hyperbolic space is a Riemannian manifold $\mathbb{H}^d = \{x \in \mathbb{R}^d : [x, x] = -1\}$ with the distance function given by $d(x, y) = \text{acosh}(-[x, y])$. Finally, 0 and 1 are all-zero and all-one vectors of appropriate dimensions. Let C be a subset of a metric space (S, d) , and $x \in S$; We define

$$d_{\min}(C) = \inf \{d(x, y) : x, y \in C, x \neq y\},$$

$$d_{\max}(x, C) = \sup \{d(x, y) : y \in C\}.$$

The cardinality of a discrete set C is denoted by $\text{card } C$. The graph-theoretic notations simplifies the main results of this paper. For a graph G , we denote its edge set as $E(G)$. Let G_{p_1, \dots, p_K} be a complete K -partite graph with part sizes p_1, \dots, p_K . The Turán graph [37] $T(N, K)$ is a complete K -partite graph with N vertices, and part sizes⁵

$$p_k = \begin{cases} N_1 + 1, & \text{for } 1 \leq k \leq K_1 \\ N_1, & \text{for } K_1 + 1 \leq k \leq K. \end{cases}$$

Then, $\text{card } E(T(N, K)) = \binom{N}{2} - K_1 \binom{N_1+1}{2} - (K - K_1) \binom{N_1}{2}$.⁶

7.1 Proof of Proposition 1

From Definition 1, the values for $\alpha_1(X)$, $\alpha_2(X)$ and $\alpha_3(X)$ are trivial. The lower bound for $\alpha_N(X)$ simply follows from the uniqueness of pairwise distances. To put formally, we have

$$\alpha_N(X) = \min_{1 \leq m \leq \binom{N}{2}} \left\{ \text{card} \bigcup_{s=1}^m \{\lambda_{1,s}, \lambda_{2,s}\} = N \right\} \geq \left\lceil \frac{N}{2} \right\rceil.$$

For the upper bound, $\alpha_N(X)$ is maximum when all $N - 1$ smallest pairwise distances are incident to a unique point; see Figure 2 (b). The total length of the distance list is $\binom{N}{2}$. Therefore, we have

$$\alpha_N(X) \leq \binom{N}{2} - (N - 1) + 1 = \binom{N - 1}{2} + 1.$$

7.2 Proof of Theorem 1

Let us separately consider hyperbolic, Euclidean, and spherical spaces.

⁵From $\sum_{k=1}^K p_k = N$, we have $N_1 = \lfloor \frac{N}{K} \rfloor$, $K_1 = N - KN_1$.

⁶This is simplified from $\text{card } E(G_{p_1, \dots, p_K}) = \binom{N}{2} - \sum_{k=1}^K \binom{p_k}{2}$. For $K > N$, we assume the graph is complete and $E(T(N, K)) = \binom{N}{2}$.

7.2.1 Hyperbolic space

Let $r \in \mathbb{R}^+$, and $x_1(r), \dots, x_N(r) \in \mathbb{L}^d$ be a set of parameterized points in 'Loid model of d -dimensional hyperbolic space with $C = -1$ (see Table 1), such that

$$x_n(r) = \begin{bmatrix} \sqrt{1 + \|y_n(r)\|^2} \\ y_n(r) \end{bmatrix}, \forall n \in [N]$$

where $y_N(r) = 0$, and $y_i(r)^\top y_j(r) = r^2 \cos 2\pi \frac{|i-j|}{N-1}, \forall i, j \in [N-1]$. To see an example, see Figure 10. For these data points, we have

$$\begin{aligned} d_{\min}(\{x_n(r)\}_{n=1}^{N-1}) &= \operatorname{acosh}\left(1 + r^2(1 - \cos \frac{2\pi}{N-1})\right), \\ d_{\max}(\{x_n(r)\}_{n=1}^{N-1}, x_N(r)) &= \operatorname{acosh}(\sqrt{1 + r^2}). \end{aligned}$$

Therefore, for any $N \in \mathbb{N}$, there exists a $r \in \mathbb{R}^+$ such that $\{x_n(r)\}_{n=1}^N \subseteq \mathbb{L}^d$. Hence,

$$\begin{aligned} K(\mathbb{L}^d) &= \sup \left\{ N : \{x_n(r)\}_{n=1}^N \subseteq \mathbb{L}^d \right\} \\ &= \infty. \end{aligned}$$

This result hold for all dimensions $d \geq 2$.

7.2.2 Euclidean space

Lemma 1. *There is a set of points x_1, \dots, x_N in \mathbb{R}^d such that*

$$\|x_n - x_N\| = 1, \forall n \in [N-1],$$

where $d_{\max}(x_N, \{x_n\}_{n=1}^{N-1}) \leq d_{\min}(\{x_n\}_{n=1}^{N-1})$ and $N = K(\mathbb{R}^d)$.

Proof. Let $\{y_n\}_{n=1}^N$ be a set of points in \mathbb{R}^d such that

$$d_{\max}(y_N, \{y_n\}_{n=1}^{N-1}) \leq d_{\min}(\{y_n\}_{n=1}^{N-1}),$$

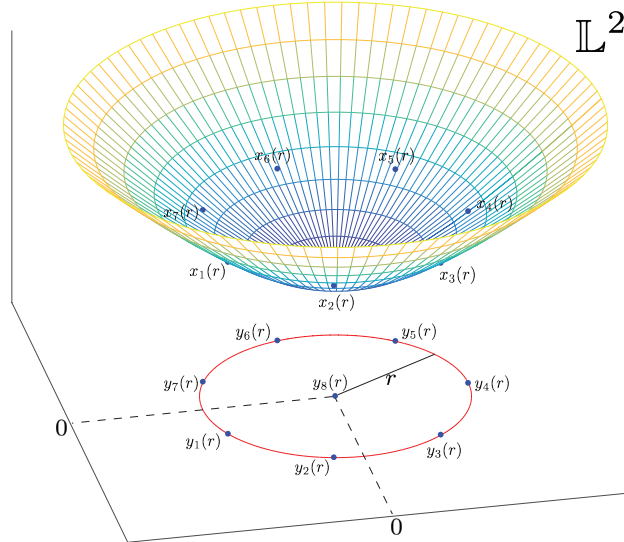


Figure 10: An example of $N = 8$ parameterized points $\{x_n(r)\}_{n=1}^N$ in \mathbb{L}^2 and $\{y_n(r)\}_{n=1}^N$ in \mathbb{R}^2 .

or $\alpha_N(\{y_n\}_{n=1}^N) = \binom{N-1}{2} + 1$. Without loss of generality, we assume $y_N = 0$ and $d_{\max}(y_N, \{y_n\}_{n=1}^{N-1}) = 1$. Let $x_n = \frac{1}{\|y_n\|} y_n$, $\forall n \in [N-1]$ and $x_N = y_N$. We want to show that $\alpha_N(\{x_n\}_{n=1}^N) \geq \alpha_N(\{y_n\}_{n=1}^N)$. Following the definition of ordinal spread, we have

$$\begin{aligned} \alpha_N(\{x_n\}_{n=1}^N) &\stackrel{(a)}{\geq} \text{card} \left\{ (i, j) : d(x_i, x_j) \geq d_{\max}(x_N, \{x_n\}_{n=1}^{N-1}), i, j \in [N-1], i > j \right\} + 1, \\ &\stackrel{(b)}{=} \text{card} \left\{ (i, j) : d(x_i, x_j) \geq 1, i, j \in [N-1], i > j \right\} + 1, \\ &\stackrel{(c)}{\geq} \text{card} \left\{ (i, j) : d(y_i, y_j) \geq 1, i, j \in [N-1], i > j \right\} + 1, \\ &= \alpha_N(\{y_n\}_{n=1}^N) \end{aligned}$$

where (a) holds with equality if x_N appears last in the sorted distance list, i.e., if $x_N = x_{(N)}$, (b) is due to $d_{\max}(x_N, \{x_n\}_{n=1}^{N-1}) = 1 = d_{\max}(y_N, \{y_n\}_{n=1}^{N-1})$. To prove inequality (c), let $d(y_i, y_j) \geq 1$ for distinct $i, j \in [N-1]$. Then,

$$\begin{aligned} d(y_i, y_j)^2 &= \frac{\|y_i\| - 1}{\|y_i\|} \left(\|y_i - y_j\|^2 - \|y_j\|^2 + \|y_i\| \right) + \left\| \frac{1}{\|y_i\|} y_i - y_j \right\|^2 \\ &= \frac{d(y_N, y_i) - 1}{\|y_i\|} (d(y_i, y_j)^2 - d(y_N, y_j)^2 + d(y_N, y_i)) + \left\| \frac{1}{\|y_i\|} y_i - y_j \right\|^2 \\ &\stackrel{(a)}{\leq} \left\| \frac{1}{\|y_i\|} y_i - y_j \right\|^2 \\ &\stackrel{(b)}{\leq} \left\| \frac{1}{\|y_i\|} y_i - \frac{1}{\|y_j\|} y_j \right\|^2 \\ &= d(x_i, x_j)^2 \end{aligned}$$

where (a) follows from $d(y_N, y_i) \leq 1$, $d(y_N, y_j) \leq 1$, $d(y_i, y_j)^2 \geq 1$, and (b) follows from the symmetry in the argument. Therefore, we have

$$\{(i, j) : d(y_i, y_j) \geq 1, i, j \in [N-1], i > j\} \subseteq \{(i, j) : d(x_i, x_j) \geq 1, i, j \in [N-1], i > j\}.$$

Hence, $\{x_n\}_{n=1}^N$ is an ordinally dense subset of \mathbb{R}^d . □

From Lemma 1, we want find an ordinally dense set of points x_1, \dots, x_N in \mathbb{R}^d such that

$$\|x_n\| = 1, n \in [N-1] \text{ and } x_N = 0.$$

From the definition of ordinal spread, we have

$$\begin{aligned} \alpha_N(\{x_n\}_{n=1}^N) &= \text{card} \left\{ (i, j) : d(x_i, x_j) \geq d_{\max}(x_N, \{x_n\}_{n=1}^{N-1}), i, j \in [N-1], i > j \right\} + 1, \\ &= \text{card} \left\{ (i, j) : \|x_i\|^2 + \|x_j\|^2 - 2x_i^\top x_j \geq 1^2, i, j \in [N-1], i > j \right\} + 1, \\ &= \text{card} \left\{ (i, j) : \text{acos}(x_i^\top x_j) \geq \frac{\pi}{3}, i, j \in [N-1], i > j \right\} + 1. \end{aligned}$$

We can find a maximum number of ordinally dense points by solving a spherical cap packing problem; see Figure 11.

Definition 5. Let \mathbb{S}^{d-1} be the $(d-1)$ -dimensional unit sphere in \mathbb{R}^d . We define the spherical α -cap $C_x(\alpha)$ as

$$C_x(\alpha) = \{y \in \mathbb{S}^{d-1} : x^\top y < \cos(\alpha)\},$$

for any $x \in \mathbb{S}^{d-1}$.

Definition 6. The maximum number of non-overlapping $C_x(\alpha)$ is defined as

$$N(\alpha) = \max_{N \in \mathbb{N}} \left\{ N : \exists x_1, \dots, x_N \in \mathbb{S}^{d-1} \text{ such that } \bigcup_{j \in \mathcal{I}, j \neq i} C_{x_j}(\alpha) \cap C_{x_i}(\alpha) = \emptyset, \forall \mathcal{I} \subseteq [N], \forall i \in [N] \right\}.$$

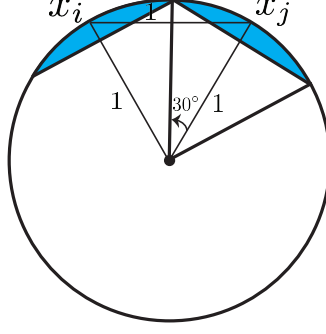


Figure 11: Spherical $\frac{\pi}{6}$ -cap packing on the surface of a unit sphere \mathbb{S}^1 .

Therefore, we have

$$\begin{aligned}
 K(\mathbb{R}^d) &= \sup \left\{ \text{card} \{x_n\} : \{x_n\} \subseteq \mathbb{R}^d \right\}, \\
 &= \sup \left\{ N : x_1, \dots, x_N \in \mathbb{R}^d, \alpha_N(\{x_n\}_{n=1}^N) = \binom{N-1}{2} + 1 \right\}, \\
 &= \sup \left\{ N : x_1, \dots, x_N \in \mathbb{R}^d, \text{card} \left\{ (i, j) : \text{acos}(x_i^\top x_j) \geq \frac{\pi}{3}, i, j \in [N-1], i > j \right\} = \binom{N-1}{2} \right\}, \\
 &= \sup \left\{ N : x_1, \dots, x_N \in \mathbb{R}^d \text{ such that } \text{acos}(x_i^\top x_j) \geq \frac{\pi}{3}, i, j \in [N], i \neq j \right\} + 1, \\
 &\stackrel{(a)}{=} N\left(\frac{\pi}{6}\right) + 1, \\
 &\stackrel{(b)}{\leq} \left\lfloor \sqrt{\frac{\pi}{8}} \frac{\Gamma\left(\frac{d-1}{2}\right)}{\Gamma\left(\frac{d}{2}\right) \int_0^{\frac{\pi}{4}} \sin^{d-2} \theta \left(\cos \theta - \frac{\sqrt{2}}{2}\right) d\theta} \right\rfloor + 1,
 \end{aligned}$$

where (a) follows from a simple illustration in Figure 11, and (b) is given in [29]. For large d , Rankin provided the following approximation,

$$N(\alpha) \sim \frac{(\frac{1}{2}\pi d^3 \cos 2\alpha)^{\frac{1}{2}}}{(\sqrt{2} \sin \alpha)^{d-1}}.$$

Therefore, we have $N(\frac{\pi}{6}) \sim \sqrt{\pi} d^{\frac{3}{2}} 2^{\frac{d-3}{2}} = O(2^{\frac{d+3 \log d}{2}})$. The maximum number of non-overlapping spherical caps of half angle θ which can be placed on the unit sphere in \mathbb{R}^d is not less than $\exp(-d \log \sin 2\theta + o(d))$ [42]. Therefore, the lower bound on $N(\frac{\pi}{6})$ is given by $\exp(-d \log \frac{\sqrt{3}}{2} + o(d))$.

The centers of spherical caps in \mathbb{R}^2 form a regular hexagon; see Figure 2 (b). Therefore, we have $K(\mathbb{R}^2) = 6 + 1 = 7$. However, these spherical caps overlap each other at exactly one point. Hence, the number of strictly non-overlapping spherical caps in \mathbb{R}^2 is 5. This leads to the pentagon configuration in Figure 4 (b).

7.2.3 Spherical space

Lemma 2. *There is a set of points x_1, \dots, x_N in \mathbb{S}^d such that*

$$d(x_n, x_N) = \text{acos}(1 - \epsilon), \forall n \in [N-1],$$

where $d_{\max}(x_N, \{x_n\}_{n=1}^{N-1}) \leq d_{\min}(\{x_n\}_{n=1}^{N-1})$, $N = K(\mathbb{S}^d)$, and for some $\epsilon \geq 0$.

Proof. Let $\{y_n\}_{n=1}^N$ be a set of points in \mathbb{S}^d such that

$$d_{\max}(y_N, \{y_n\}_{n=1}^{N-1}) \leq d_{\min}(\{y_n\}_{n=1}^{N-1}),$$

or $\alpha_N(\{y_n\}_{n=1}^N) = \binom{N-1}{2} + 1$. Without loss of generality, we assume $\alpha_N(\{y_n\}_{n=1}^N) = \binom{N-1}{2} + 1$, $y_N = e_1$,⁷ and

⁷ e_1 is the first standard base vector for \mathbb{R}^{d+1} .

$d_{\max}(y_N, \{y_n\}_{n=1}^{N-1}) = \text{acos}(1 - \epsilon)$. From the latter condition, we have

$$y_n \stackrel{\text{def}}{=} \begin{bmatrix} \sqrt{1 - \|z_n\|^2} \\ z_n \end{bmatrix}, \text{ such that } \|z_n\| \leq \sqrt{1 - (1 - \epsilon)^2}.$$

Let us define

$$x_n = \begin{bmatrix} 1 - \epsilon \\ \sqrt{1 - (1 - \epsilon)^2} \frac{1}{\|z_n\|} z_n \end{bmatrix}, \forall n \in [N - 1]$$

and $x_N = e_1$. Then, we claim $\alpha_N(\{x_n\}_{n=1}^N) \geq \alpha_N(\{y_n\}_{n=1}^N)$. Following the definition of ordinal spread, we have

$$\begin{aligned} \alpha_N(\{x_n\}_{n=1}^N) &\stackrel{(a)}{=} \text{card} \left\{ (i, j) : d(x_i, x_j) \geq d_{\max}(x_N, \{x_n\}_{n=1}^{N-1}), i, j \in [N - 1], i > j \right\} + 1, \\ &\stackrel{(b)}{=} \text{card} \left\{ (i, j) : d(x_i, x_j) \geq \text{acos}(1 - \epsilon), i, j \in [N - 1], i > j \right\} + 1, \\ &\stackrel{(c)}{\geq} \text{card} \left\{ (i, j) : d(y_i, y_j) \geq \text{acos}(1 - \epsilon), i, j \in [N - 1], i > j \right\} + 1, \\ &= \alpha_N(\{y_n\}_{n=1}^N), \end{aligned}$$

where (a) holds with equality if x_N appears last in the sorted distance list, (b) is due to $d_{\max}(x_N, \{x_n\}_{n=1}^{N-1}) = \text{acos}(1 - \epsilon) = d_{\max}(y_N, \{y_n\}_{n=1}^{N-1})$. For inequality (c), let $d(y_i, y_j) \geq \text{acos}(1 - \epsilon)$ for distinct $i, j \in [N - 1]$ and $z_i^\top z_j = \|z_i\| \|z_j\| \cos \theta_{ij}$. Therefore,

$$\begin{aligned} \cos \theta_{ij} &= \frac{1}{\|z_i\| \|z_j\|} z_i^\top z_j \\ &\stackrel{(a)}{\leq} \frac{1}{\|z_i\| \|z_j\|} \left(1 - \epsilon - \sqrt{1 - \|z_i\|^2} \sqrt{1 - \|z_j\|^2} \right) \\ &\stackrel{(b)}{\leq} 0. \end{aligned}$$

where (a) is due to

$$y_i^\top y_j = \sqrt{1 - \|z_i\|^2} \sqrt{1 - \|z_j\|^2} + z_i^\top z_j \leq 1 - \epsilon,$$

and inequality (b) is due $\sqrt{1 - \|z_i\|^2} \geq \sqrt{1 - \sqrt{1 - (1 - \epsilon)^2}^2} = \sqrt{1 - \epsilon^2}$.⁸ Then, we have

$$\begin{aligned} d(x_i, x_j) &= \text{acos} \left((1 - \epsilon)^2 + (1 - (1 - \epsilon)^2) \cos \theta_{ij} \right) \\ &\geq \text{acos} \left(\sqrt{1 - \|z_i\|^2} \sqrt{1 - \|z_j\|^2} + z_i^\top z_j \right) \\ &= d(y_i, y_j) \end{aligned}$$

since $(1 - (1 - \epsilon)^2) \cos \theta_{ij} \leq \|z_i\| \|z_j\| \cos \theta_{ij}$ where $\cos \theta_{ij} \leq 0$. Therefore, we have

$$\{(i, j) : d(y_i, y_j) \geq \text{acos}(1 - \epsilon), i, j \in [N - 1], i > j\} \subseteq \{(i, j) : d(x_i, x_j) \geq \text{acos}(1 - \epsilon), i, j \in [N - 1], i > j\}.$$

Hence, $\{x_n\}_{n=1}^N$ is an ordinally dense subset of \mathbb{S}^d . \square

Now, let us find ordinally dense set of points x_1, \dots, x_N in \mathbb{S}^d with

$$x_n = \begin{bmatrix} 1 - \epsilon \\ z_n \end{bmatrix}, \forall n \in [N - 1] \text{ and } x_N = e_1.$$

⁸Similarly, we have $\sqrt{1 - \|z_j\|^2} \geq \sqrt{1 - \epsilon^2}$.

We have $\|z_n\|^2 = 1 - (1 - \epsilon)^2$ for all $\forall n \in [N - 1]$. We begin from the definition of ordinal spread as follows

$$\begin{aligned} \alpha_N(\{x_n\}_{n=1}^N) &= \text{card} \left\{ (i, j) : d(x_i, x_j) \geq d_{\max}(x_N, \{x_n\}_{n=1}^{N-1}), i, j \in [N - 1], i > j \right\} + 1, \\ &= \text{card} \left\{ (i, j) : d(x_i, x_j) \geq \text{acos}(1 - \epsilon), i, j \in [N - 1], i > j \right\} + 1, \\ &= \text{card} \left\{ (i, j) : \frac{1}{\|z_i\| \|z_j\|} z_i^\top z_j \leq \frac{\epsilon(1 - \epsilon)}{1 - (1 - \epsilon)^2}, i, j \in [N - 1], i > j \right\} + 1, \\ &= \text{card} \left\{ (i, j) : \text{acos}(\widehat{z}_i^\top \widehat{z}_j) \geq \frac{\pi}{3}, i, j \in [N - 1], i > j \right\} + 1, \end{aligned}$$

where $\widehat{z}_i = \frac{1}{\|z_i\|} z_i$, $\widehat{z}_j = \frac{1}{\|z_j\|} z_j$, and $\sup_{\epsilon} \frac{\epsilon(1 - \epsilon)}{1 - (1 - \epsilon)^2} = \frac{1}{2}$. Similar to the Euclidean space, this problem is equivalent to spherical $\frac{\pi}{6}$ -cap packing number in \mathbb{R}^d , since $\widehat{z}_n \in \mathbb{R}^d$. Finally, if we assume $\min_{i, j \in [N], i > j} d(x_i, x_j) = \delta$, we have $d_{\max}(x_N, \{x_n\}_{n=1}^{N-1}) \geq \delta$. Therefore, the cap angles can be computed as follows

$$\alpha = \min_{\epsilon \geq 1 - \cos \delta} \frac{1}{2} \text{acos} \frac{\epsilon(1 - \epsilon)}{1 - (1 - \epsilon)^2} = \frac{1}{2} \text{acos} \frac{\cos \delta}{1 + \cos \delta} > \frac{\pi}{6}.$$

In this case, the ordinal capacity can be refined as spherical α -cap packing number.

7.3 Proof of Theorem 2

Let S be a d -dimensional space form, and $N \leq K(S)$. From Definition 4, we can find an ordinaly dense subset $x_1, \dots, x_N \in S$. Hence, we have

$$\begin{aligned} A_N(S) &= \sup_{x_1, \dots, x_N \in S} \alpha_N(\{x_n\}_{n=1}^N), \\ &\stackrel{(a)}{=} \binom{N - 1}{2} + 1 \end{aligned}$$

where (a) directly follows from Proposition 1. This is the number of edges of a complete graph with $N - 1$ vertices plus one.

Now, let us consider $N > K(S)$. This could only happen in (d -dimensional) Euclidean and spherical spaces, since hyperbolic spaces have infinite ordinal capacity, i.e., $K(\mathbb{H}^d) = \infty$.

In Section 7.2, we proved that there is a set of points $x_1, \dots, x_{N-1} \in \mathbb{R}^d$ on the unit sphere and $x_N = 0$ such that

$$\begin{aligned} A_N(S) &= \alpha_N(\{x_n\}_{n=1}^N), \\ &= \text{card} \{(i, j) : d(x_i, x_j) \geq 1, i, j \in [N - 1], i > j\} + 1. \end{aligned}$$

Consider a pair of points $x_i, x_j \in \mathbb{R}^d$ with $d(x_i, x_j) < 1$. We can move the point x_i and place it on x_j if

$$\text{card} \{(i, k) : d(x_i, x_k) \geq 1, i, k \in [N - 1], i \neq k\} \leq \text{card} \{(j, k) : d(x_j, x_k) \geq 1, j, k \in [N - 1], j \neq k\}.$$

This condition is to ensure that we do not decrease $\alpha_N(\{x_n\}_{n=1}^N)$. We repeat this process and lump the set of $N - 1$ point on $K < N - 1$ positions, i.e., p_1, \dots, p_K . At each position p_k , we place multiple vertices. Finally, $\alpha_N(\{x_n\}_{n=1}^N)$ is equal to the number of edges – with length greater than 1 – in this K -partite graph with $N - 1$ vertices. This graph is K -partite because the distance between points in a partition have distances of zero. Hence, their edges do not contribute in calculating the ordinal spread of the point set. This graph becomes a complete K -partite graph if all distinct positions $\{p_k\}$ belong to the centers of spherical $\frac{\pi}{6}$ -caps on the unit sphere. On the other hand, the number of edges in a complete K -partite graph is maximized when the size of the parts differs by at most one, i.e., Turán graph $T(N - 1, K)$ [37]. Therefore, the N -point ordinal spread of S (Euclidean or spherical space) is given by

$$A_N(S) = \text{card } E(T(N - 1, K(S) - 1)) + 1.$$

The maximum number of possible partitions $(K(S) - 1)$ gives the maximum number of edges, i.e.,

$$\text{card } E(T(N - 1, 1)) \leq \text{card } E(T(N - 1, 2)) \leq \dots \leq \text{card } E(T(N - 1, K(S) - 1)).$$

This completes the proof.

8 NUMERICAL EXPERIMENTS

8.1 Distance Comparisons Reveal Hyperbolicity of Trees

We generate random weighted trees with $N = 10^4$ nodes. The edge weights are drawn from i.i.d. uniform distribution in $[0, 1]$. The distance between each two nodes is the weight of the path joining them. We contaminate the corresponding distance matrix by an additive zero mean Gaussian noise with the signal to noise ratio of 40 dB. In this experiment, we consider three different trees with maximum degrees of 4, 5, 6.⁹ In Figure 12, we show the distribution of node degrees for each tree.

8.1.1 Statistical Test

We generate random points in space forms of dimension $d = 2, \dots, 5$, from the following distributions

- Hyperbolic space: $x = [\sqrt{1 + \|z\|^2}, z^\top]^\top$, where $z \sim \mathcal{N}(0, \sigma^2 I)$ and $\sigma = 100$;
- Euclidean space: $x \sim \mathcal{N}(0, \sigma^2 I)$;
- Spherical space: $x = \frac{1}{\|z\|} z$, where $z \sim \mathcal{N}(0, \sigma^2 I)$.¹⁰

The statistics of the ordinal spread variables are *invariant* with respect isotonic transformation of data points, e.g., rotation, translation, and uniform scaling in Euclidean space. Therefore, we can also use compact distributions, e.g., the multivariate uniform distribution. The arbitrary choices of Gaussian and uniform distributions do not significantly change the statistics of the ordinal spread variables — at least, it does not affect the key results in this experiment.

Commonly, in embedding trees, the leaves concentrate near the boundary of the Poincaré disk. Hence, we choose a large variance σ to heavily sample the points closer to the boundary of Poincaré disk; see Figure 5 (a). Finally, we devise a hypothesis test based on the total variation distance of probability measures, i.e.,¹¹

$$\delta(P, Q) = \|P - Q\|_1.$$

For each tree T with $\Delta(T) = 4, 5$ and 6, we report the distances between the target (oracle) and empirical probability mass functions (PMF) of $\alpha_{k,N}$ for points generated in each space form. In Tables 4 to 6, we consider sub-cliques — randomly sampled from each tree — with $N = 20$ nodes. From the hypothesis tests for $\alpha_{k,N}$, $k \in \{3, \dots, 20\}$, we conclude that the ordinal spread variables of random trees better match with hyperbolic ordinal spread variables.

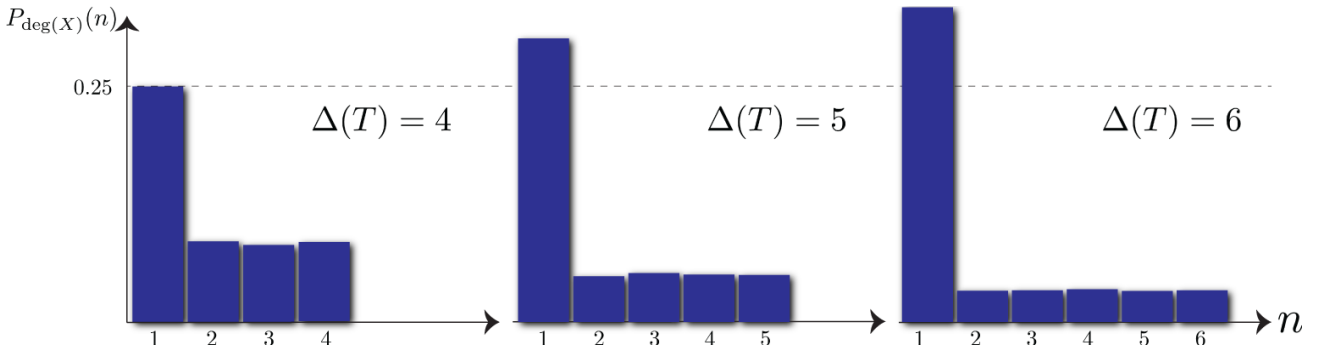


Figure 12: The distribution of node degrees for each random tree.

⁹In the main manuscript, we have mistakenly denoted them as $\Delta(T) = 3, 4, 5$.

¹⁰Therefore, the points are distributed uniformly on \mathbb{S}^d .

¹¹The total variation distance is $\delta(P, Q) = \frac{1}{2} \|P - Q\|_1$, but we can ignore the constant term.

Geometry of Comparisons

Table 4: $\delta(P_{\alpha_{k,N}}^S, \hat{P}_{\alpha_{k,N}}) \times 10^{-3}$ for different space forms — $\Delta(T) = 4$.

k	3	4	5	6	7	8	9	10	11	12	13	14	15	16	17	18	19	20
\mathbb{L}^2	0	1.6	1.9	1.7	1.8	2.1	2.4	2.5	2.3	2.1	2.1	2.0	2.0	2.1	2.2	2.3	2.4	2.2
\mathbb{L}^3	0	2.3	2.8	2.5	2.4	2.5	2.9	3.0	2.9	2.6	2.5	2.3	2.2	2.0	1.9	1.8	1.8	1.7
\mathbb{L}^4	0	2.7	3.3	3.0	2.8	2.8	3.0	3.2	3.3	3.0	2.8	2.6	2.4	2.2	2.0	1.7	1.5	1.3
\mathbb{L}^5	0	3.0	3.6	3.4	3.0	3.1	3.2	3.4	3.5	3.3	3.0	2.8	2.6	2.3	2.1	1.8	1.5	1.1
\mathbb{R}^2	0	1.5	1.9	2.1	2.4	2.8	2.9	3.1	3.2	3.3	3.4	3.5	3.7	3.9	4.2	4.7	5.4	6.7
\mathbb{R}^3	0	2.2	2.7	2.6	2.8	3.4	3.5	3.7	3.7	3.8	3.9	4.0	4.1	4.1	4.3	4.5	4.9	5.9
\mathbb{R}^4	0	2.6	3.2	3.1	3.1	3.6	3.8	3.9	4.0	4.1	4.2	4.3	4.3	4.3	4.3	4.4	4.7	5.4
\mathbb{R}^5	0	2.8	3.5	3.5	3.3	3.8	3.9	4.1	4.1	4.2	4.4	4.4	4.4	4.3	4.3	4.4	4.6	5.1
\mathbb{S}^2	0	8.4	9.9	10.2	10.1	10	9.9	9.8	9.6	9.2	8.7	8.6	8.6	8.6	8.5	8.5	8.5	8.8
\mathbb{S}^3	0	8.4	9.8	10.2	10.1	10.1	10	9.9	9.6	9.3	8.8	8.7	8.7	8.7	8.7	8.7	8.7	8.8
\mathbb{S}^4	0	8.4	9.8	10.1	10.2	10.1	10	9.9	9.7	9.4	8.9	8.8	8.8	8.8	8.8	8.8	8.8	8.8
\mathbb{S}^5	0	8.5	9.8	10.1	10.2	10.1	10.1	9.9	9.7	9.4	8.9	8.9	8.9	8.9	8.8	8.8	8.8	8.7

Table 5: $\delta(P_{\alpha_{k,N}}^S, \hat{P}_{\alpha_{k,N}}) \times 10^{-3}$ for different space forms — $\Delta(T) = 5$.

k	3	4	5	6	7	8	9	10	11	12	13	14	15	16	17	18	19	20
\mathbb{L}^2	0	1.6	2.0	2.6	2.8	2.8	2.8	2.6	2.6	2.5	2.4	2.2	2.1	1.9	1.7	1.4	1.1	0.7
\mathbb{L}^3	0	2.3	2.8	3.1	3.4	3.5	3.5	3.5	3.3	3.3	3.1	3.0	2.8	2.6	2.3	2.0	1.5	0.8
\mathbb{L}^4	0	2.7	3.3	3.4	3.7	3.9	3.9	3.9	3.8	3.7	3.6	3.5	3.3	3.1	2.8	2.5	2.0	1.2
\mathbb{L}^5	0	3.0	3.6	3.6	3.8	4.2	4.2	4.2	4.2	4.0	3.9	3.8	3.6	3.4	3.1	2.8	2.3	1.6
\mathbb{R}^2	0	1.5	2.3	3.4	3.6	4.0	4.2	4.4	4.6	4.8	5.0	5.3	5.6	5.9	6.3	6.9	7.5	8.4
\mathbb{R}^3	0	2.2	2.7	3.8	4.2	4.6	4.8	5.0	5.1	5.2	5.4	5.6	5.8	6.0	6.3	6.7	7.1	7.8
\mathbb{R}^4	0	2.6	3.2	3.9	4.5	4.9	5.0	5.2	5.4	5.5	5.6	5.8	5.9	6.1	6.3	6.6	6.9	7.3
\mathbb{R}^5	0	2.8	3.5	4.1	4.6	5.0	5.2	5.4	5.5	5.7	5.8	5.9	6.0	6.1	6.3	6.5	6.7	7.0
\mathbb{S}^2	0	8.4	9.9	10.2	10.1	10	9.9	9.8	9.6	9.5	9.5	9.5	9.5	9.5	9.5	9.5	9.6	9.7
\mathbb{S}^3	0	8.4	9.8	10.2	10.1	10.1	10	9.9	9.6	9.5	9.6	9.6	9.6	9.6	9.7	9.7	9.7	9.7
\mathbb{S}^4	0	8.4	9.8	10.1	10.2	10.1	10	9.9	9.7	9.6	9.6	9.7	9.7	9.7	9.7	9.8	9.8	9.7
\mathbb{S}^5	0	8.5	9.8	10.1	10.2	10.1	10.1	9.9	9.7	9.7	9.7	9.7	9.7	9.8	9.8	9.8	9.8	9.7

Table 6: $\delta(P_{\alpha_{k,N}}^S, \hat{P}_{\alpha_{k,N}}) \times 10^{-3}$ for different space forms — $\Delta(T) = 6$.

k	3	4	5	6	7	8	9	10	11	12	13	14	15	16	17	18	19	20
\mathbb{L}^2	0	1.6	2.5	3.0	3.2	3.2	3.1	2.9	2.9	2.7	2.5	2.3	2.1	1.9	1.6	1.3	1.1	1.4
\mathbb{L}^3	0	2.3	2.8	3.6	3.8	3.8	3.8	3.7	3.6	3.5	3.3	3.0	2.8	2.5	2.1	1.6	1.0	0.8
\mathbb{L}^4	0	2.7	3.3	3.9	4.0	4.2	4.2	4.2	4.0	3.9	3.7	3.5	3.2	2.9	2.5	1.9	1.2	0.4
\mathbb{L}^5	0	3.0	3.6	4.0	4.2	4.5	4.5	4.4	4.3	4.1	4.0	3.8	3.5	3.2	2.8	2.2	1.5	0.5
\mathbb{R}^2	0	1.5	2.8	3.8	4.0	4.3	4.5	4.6	4.7	4.9	5.0	5.2	5.4	5.6	5.8	6.2	6.7	7.5
\mathbb{R}^3	0	2.2	3.0	4.2	4.5	4.9	5.0	5.2	5.3	5.3	5.4	5.5	5.6	5.7	5.8	6.0	6.2	6.8
\mathbb{R}^4	0	2.6	3.2	4.4	4.8	5.2	5.3	5.4	5.5	5.6	5.6	5.7	5.7	5.8	5.8	5.9	6.0	6.3
\mathbb{R}^5	0	2.8	3.5	4.5	5.0	5.3	5.4	5.6	5.7	5.7	5.8	5.8	5.8	5.8	5.8	5.8	5.8	5.9
\mathbb{S}^2	0	8.4	9.9	10.2	10.1	10	9.9	9.8	9.6	9.4	9.4	9.4	9.4	9.3	9.3	9.3	9.2	9.3
\mathbb{S}^3	0	8.4	9.8	10.2	10.1	10.1	10	9.9	9.6	9.5	9.5	9.5	9.5	9.5	9.5	9.4	9.4	9.3
\mathbb{S}^4	0	8.4	9.8	10.1	10.2	10.1	10	9.9	9.7	9.6	9.6	9.6	9.6	9.5	9.5	9.5	9.4	9.3
\mathbb{S}^5	0	8.5	9.8	10.1	10.2	10.1	10.1	9.9	9.7	9.6	9.6	9.6	9.6	9.6	9.6	9.5	9.5	9.3

Ordinal spread variables of larger sub-cliques are more effective in testing for distinguishing the curvature sign and the dimension of space forms. For instance, consider a triangle in a space form. Regardless of the presumed space form, we have

$$\alpha_{k,3} = \begin{cases} 1 & \text{if } k = 1, \\ 1 & \text{if } k = 2, \\ 2 & \text{if } k = 3, \end{cases} \quad \text{with probability 1.}$$

This is a trivial result from **Proposition 1**. Therefore, the statistics of $\alpha_{k,3}$ can not bear any useful information about the geometry of data. This fact, along with the total number of available unique sub-cliques, should be considered for implementing a proper hypothesis test based on a majority vote; see Tables 4 to 6.

Alternatively, we can design an aggregate hypothesis test based on α_N by defining the following distance function between $P_{\alpha_N}^S$ and \hat{P}_{α_N} , e.g., $\delta(P_{\alpha_N}^S, \hat{P}_{\alpha_N}) = \sum_{k=1}^N \delta(P_{\alpha_{k,N}}^S, \hat{P}_{\alpha_{k,N}})$. This definition involves all ordinal spread variables related to sub-cliques of size N , i.e., $\alpha_{k,N}$. Now, we can perform minimum-distance hypothesis tests for sub-cliques of sizes $N \in \{5, \dots, 20\}$. For each experiment, hyperbolic spaces provide the best matches for ordinal spread variables of each random tree; see Tables 7 to 9.

An important observation is that higher dimensional of space forms do not necessarily give better matches for the statistics of empirical ordinal spread variables. This is counter intuitive since we know high-dimensional spaces should be more capable to embed metric graphs compared to low-dimensional spaces. In Section 5.2, we discuss this issue and distinguish between the embedding capability of a space form versus low-dimensional approximation of data space. Finally, in absence of any prior information for proper distributions of data points, the estimate for the dimension of underlying space form is unreliable.

Table 7: $\delta(P_{\alpha_N}^S, \hat{P}_{\alpha_N}) \times 10^{-2}$ for different space forms — $\Delta(T) = 4$.

N	5	6	7	8	9	10	11	12	13	14	15	16	17	18	19	20
\mathbb{L}^2	3.3	3.7	3.9	4.1	4.2	4.2	4.1	4.1	4.0	4.0	3.9	3.8	3.8	3.7	3.6	3.6
\mathbb{L}^3	3.0	3.8	4.2	4.6	4.7	4.7	4.7	4.6	4.6	4.5	4.4	4.4	4.3	4.2	4.1	4.0
\mathbb{L}^4	3.4	4.1	4.7	5.0	5.2	5.2	5.1	5.1	5.0	4.9	4.8	4.8	4.7	4.5	4.4	4.4
\mathbb{L}^5	3.7	4.4	5.0	5.3	5.5	5.5	5.5	5.4	5.3	5.3	5.2	5.1	5.0	4.9	4.8	4.7
\mathbb{R}^2	7.0	8.0	8.3	8.4	8.2	8.0	7.8	7.6	7.3	7.1	6.8	6.6	6.4	6.2	6.0	5.9
\mathbb{R}^3	5.9	6.9	7.9	8.1	8.0	7.9	7.9	7.8	7.6	7.5	7.3	7.1	6.9	6.7	6.6	6.4
\mathbb{R}^4	5.2	6.6	7.6	7.9	7.9	7.9	8.0	8.0	7.8	7.7	7.5	7.3	7.2	7.0	6.9	6.7
\mathbb{R}^5	5.0	6.4	7.4	7.8	7.9	8.0	8.1	8.1	8.0	7.8	7.6	7.5	7.4	7.2	7.1	6.9
\mathbb{S}^2	12.0	15.5	17.8	19.4	20.2	20.3	20.2	19.8	19.3	18.8	18.3	17.7	17.1	16.6	16.1	15.6
\mathbb{S}^3	11.8	15.5	17.8	19.5	20.2	20.4	20.3	19.9	19.5	18.9	18.4	17.9	17.3	16.8	16.2	15.7
\mathbb{S}^4	11.7	15.4	17.8	19.5	20.1	20.4	20.3	20.0	19.6	19.0	18.5	17.9	17.4	16.9	16.3	15.8
\mathbb{S}^5	11.6	15.4	17.8	19.4	20.1	20.4	20.4	20.0	19.6	19.1	18.6	18.0	17.5	16.9	16.4	15.9

Table 8: $\delta(P_{\alpha_N}^S, \hat{P}_{\alpha_N}) \times 10^{-2}$ for different space forms — $\Delta(T) = 5$.

N	5	6	7	8	9	10	11	12	13	14	15	16	17	18	19	20
\mathbb{L}^2	5.4	5.5	5.3	5.4	5.2	5.1	4.9	4.8	4.5	4.4	4.2	4.1	3.9	3.8	3.7	3.6
\mathbb{L}^3	4.5	4.8	5.4	5.9	5.9	5.9	5.8	5.7	5.5	5.4	5.3	5.2	5.1	4.9	4.8	4.7
\mathbb{L}^4	4.1	5.0	5.9	6.3	6.4	6.4	6.4	6.3	6.2	6.2	6.1	5.9	5.8	5.7	5.5	5.4
\mathbb{L}^5	4.2	5.2	6.2	6.6	6.8	6.8	6.8	6.8	6.8	6.7	6.6	6.4	6.3	6.2	6.1	5.9
\mathbb{R}^2	9.3	10.8	11.5	11.5	11.3	11.1	10.9	10.7	10.3	10	9.7	9.4	9.1	8.9	8.6	8.4
\mathbb{R}^3	8.0	9.6	10.6	11.0	11.0	11.1	11.0	10.8	10.5	10.3	10.0	9.7	9.5	9.3	9.0	8.8
\mathbb{R}^4	7.4	9.0	10.3	10.8	10.9	11.0	11.0	10.8	10.6	10.4	10.1	9.9	9.7	9.5	9.3	9.1
\mathbb{R}^5	6.9	8.7	10.1	10.6	10.8	10.9	10.9	10.8	10.6	10.4	10.2	10.0	9.8	9.6	9.4	9.2
\mathbb{S}^2	13.6	17.2	19.6	21.0	21.7	21.8	21.6	21.2	20.6	20.0	19.4	18.8	18.1	17.5	16.9	16.4
\mathbb{S}^3	13.4	17.3	19.8	21.1	21.8	21.9	21.8	21.3	20.8	20.2	19.6	18.9	18.3	17.7	17.1	16.5
\mathbb{S}^4	13.3	17.3	19.8	21.1	21.8	22.0	21.8	21.4	20.9	20.3	19.7	19.0	18.4	17.8	17.1	16.6
\mathbb{S}^5	13.1	17.3	19.7	21.1	21.9	22.0	21.8	21.5	20.9	20.3	19.7	19.0	18.4	17.8	17.2	16.6

Table 9: $\delta(P_{\alpha_N}^S, \hat{P}_{\alpha_N}) \times 10^{-2}$ for different space forms — $\Delta(T) = 6$.

N	5	6	7	8	9	10	11	12	13	14	15	16	17	18	19	20
\mathbb{L}^2	5.8	5.8	5.9	5.8	5.7	5.5	5.2	5.0	4.9	4.7	4.6	4.4	4.3	4.2	4.1	3.9
\mathbb{L}^3	4.8	5.2	5.7	5.9	6.1	6.1	5.9	5.8	5.7	5.5	5.4	5.3	5.2	5.0	4.9	4.8
\mathbb{L}^4	4.5	5.0	5.9	6.4	6.6	6.5	6.4	6.3	6.3	6.2	6.0	5.9	5.8	5.6	5.5	5.4
\mathbb{L}^5	4.3	5.1	6.2	6.7	6.9	6.9	6.8	6.7	6.7	6.6	6.5	6.3	6.2	6.1	6.0	5.8
\mathbb{R}^2	9.6	11.1	11.7	11.7	11.4	11.1	10.8	10.5	10.2	9.9	9.6	9.3	9.0	8.7	8.5	8.3
\mathbb{R}^3	8.3	9.9	10.8	11.0	10.9	10.9	10.8	10.6	10.4	10.1	9.8	9.6	9.3	9.1	8.9	8.7
\mathbb{R}^4	7.7	9.2	10.3	10.7	10.8	10.8	10.8	10.6	10.4	10.2	10.0	9.7	9.5	9.3	9.1	8.9
\mathbb{R}^5	7.2	8.8	10.0	10.5	10.6	10.8	10.8	10.6	10.4	10.2	10.0	9.8	9.6	9.4	9.2	9.0
\mathbb{S}^2	13.3	17.0	19.3	20.6	21.3	21.4	21.2	20.8	20.3	19.7	19.1	18.5	17.9	17.3	16.7	16.2
\mathbb{S}^3	13.1	17.1	19.4	20.7	21.4	21.5	21.4	20.9	20.5	19.9	19.3	18.7	18.0	17.4	16.9	16.3
\mathbb{S}^4	13.0	17.1	19.4	20.7	21.4	21.6	21.4	21.0	20.5	20.0	19.4	18.7	18.1	17.5	16.9	16.4
\mathbb{S}^5	12.9	17.1	19.4	20.7	21.4	21.6	21.5	21.1	20.6	20.0	19.4	18.8	18.2	17.6	17.0	16.4

8.2 Single-cell Transcriptomic Data

We use the single-cell RNA sequencing atlas provided in [27]. This atlas contains 26000 cell expression vectors for adult planarians. Each cell is a 21000-dimensional integer-valued vector representing read counts of gene expressions. Therefore, this raw data reside in a 21000-dimensional Euclidean space, e.g., \mathbb{R}^{21000} . However, the specific choices of pre-processing method and the comparison criteria *imply* a geometry — namely, geometry of comparisons — that is not necessarily related to the domain of data vectors. The choice of comparisons are as follows:

- **ℓ_2 distance:** The points x_i, x_j are more similar to each other than x_k, x_l if $\|x_i - x_j\|_2 \leq \|x_k - x_l\|_2$. Here, the geometry of comparisons is a 21000-dimensional Euclidean space;
- **Angles:** The points x_i, x_j are more similar than x_k, x_l if $\angle(x_i, x_j) \leq \angle(x_k, x_l)$, where

$$\angle(x_i, x_j) \stackrel{\text{def}}{=} \arccos \frac{(x_i - \mu)^\top (x_j - \mu)}{\|x_i - \mu\| \|x_j - \mu\|},$$

and $\mu = \frac{1}{N} \sum_{n \in [N]} x_n$. We use spherical distance to compare cell vectors. Therefore, the geometry of comparisons is a spherical space of dimension $21000 - 1$.

- **Relative forest accessibility (RFA) index:** For a set of points x_1, \dots, x_N , we construct the local connectivity edge set E from a symmetric k -nearest neighbor method. The relative forest accessibility matrix is a $N \times N$ doubly stochastic matrix defined as $P = (I + L)^{-1}$ where $L = D - A$ is the Laplacian matrix, $A = (A_{i,j})$ such that

$$A_{i,j} = \exp \left(- \frac{\|x_i - x_j\|^2}{2\sigma^2} \right) [(i,j) \in E],$$

where the Iverson bracket $[(i,j) \in E] = 1$ if $(i,j) \in E$ and is 0 otherwise, and D is a diagonal matrix with $D_{ii} = \sum_{j \in [N]} A_{i,j}$. The ij -th element of P is the probability of a spanning forest includes a rooted tree at x_i and is connected to x_j — a measure of similarity between x_i and x_j [21]. In this experiment, we let $\sigma = \frac{1}{\sqrt{10N^2}} \sum_{i,j \in [N]} \|x_i - x_j\|$ and ignore the hard edge assignment since the conservative choice of kernel width performs a soft edge assignment; see Figure 13 (b). For a fast implementation of $P = (I + L)^{-1}$, we approximate the weighted adjacency matrix $A \in \mathbb{R}^{N \times N}$ with a rank-500 semidefinite matrix — via a simple eigenvalue thresholding — and use Woodbury matrix identity to compute P .

The points x_i, x_j are more similar than x_k, x_l if the relative forest accessibility index $p_{i,j}$ is greater than $p_{k,l}$. The geometry of RFA comparisons is unknown.

We propose heavy-tailed distributions for oracle distributions. To confirm the validity of this choice, we generate random normal, and log-normal (a heavy-tailed distribution) of various dimensions $d = 2, \dots, 20$, and different scale parameters; see Figure 13 (a). The log-normal distributions gives a better match for the empirical distribution of $\|X - \mathbb{E}X\|$ — which we denote as a *side information*. Specifically, we generate points according to the following distributions to find the optimal dimension and scale parameter a :

- Hyperbolic space: $x = [\sqrt{1 + \|z\|^2}, z^\top]^\top$, where $z \sim e^{a\mathcal{N}(0,I)} - \mathbb{E}e^{a\mathcal{N}(0,I)}$;
- Euclidean space: $x \sim e^{a\mathcal{N}(0,I)}$;
- Spherical space: $x = \frac{1}{\|z\|}z$, where $z \sim e^{a\mathcal{N}(0,I)} - \mathbb{E}e^{a\mathcal{N}(0,I)}$.

Therefore, we approximate the distribution of RNAseq read counts by (projected) log-normal distributions in a space form. In bioinformatics, the heavy-tailed distribution of gene expression reads is a well-known fact [?].

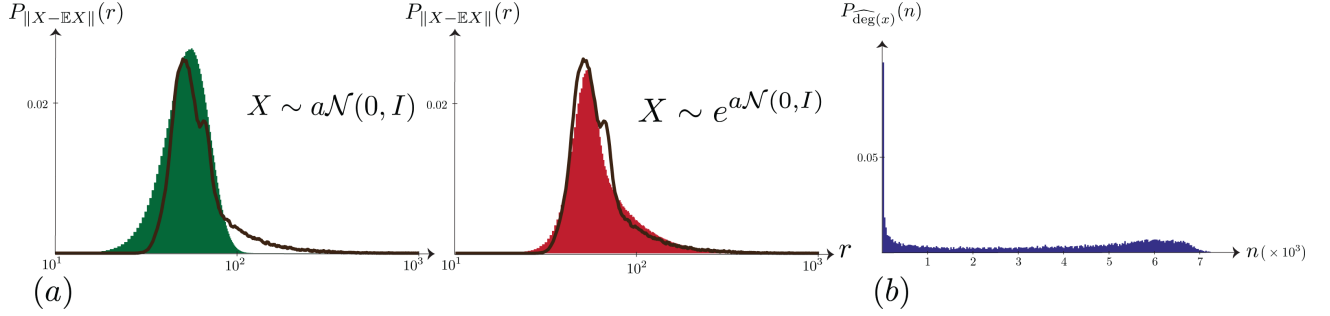


Figure 13: (a) Left: The empirical distribution of the norm of centered cell vectors (brown), and distribution of the norm of Gaussian points (green) for $d = 8$, and $a = 21.5$; (a) Right: The distribution of the norm of centered log normal points (red) for $d = 7$ and $a = 20$. (b): The distribution of *soft* degrees of each node, i.e., $\widehat{\deg}(x_n) = \sum_{m \in [N]} A_{nm}$.

ℓ_2 distances: Let $d \in \{2, 10, 10^2, 10^3, 10^4\}$, and sub-cliques of size $N = 20$. For a space form of dimension d , we iterate over a set of scale parameters a , and pick the point distribution P_x^S that produces the closest ordinal spread distribution to the empirical distribution of $\alpha_{20,20}$. We show that our proposed test detects the Euclidean space of dimension 100 as the geometry of ℓ_2 comparisons. However, higher dimensional Euclidean spaces could also be plausible choices; see Figure 14.

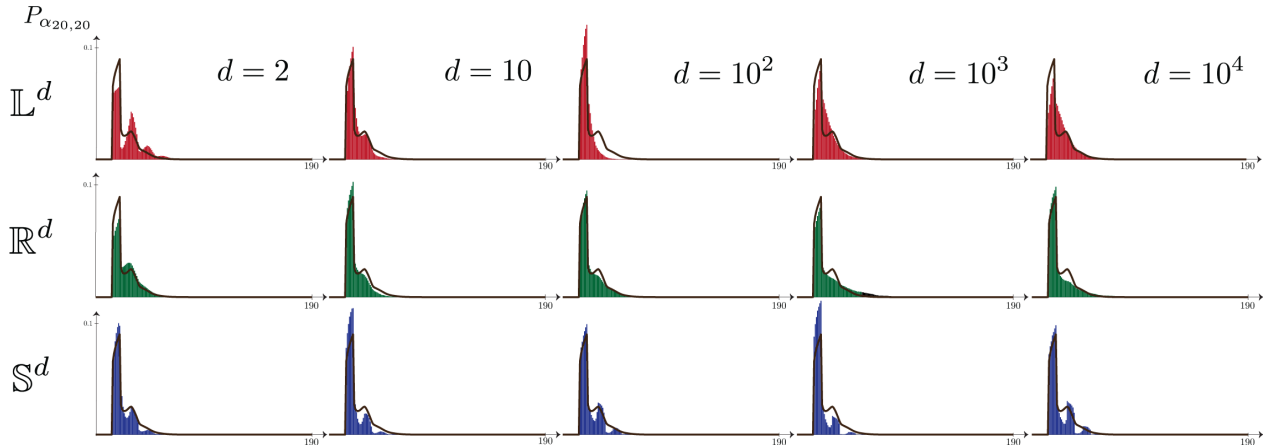


Figure 14: Brown curves represent the empirical PMF of $\alpha_{20,20}$ derived from ℓ_2 comparisons. In each row, we generate points from the corresponding space form of dimension d . This test detects a high-dimensional Euclidean space for the geometry of ℓ_2 comparisons ($d^* = 100$).

Angle comparisons: We repeat the experiment for angle comparisons explained earlier. Our proposed test identifies 10000-dimensional spherical space as the geometry of angle comparisons; see Figure 15.

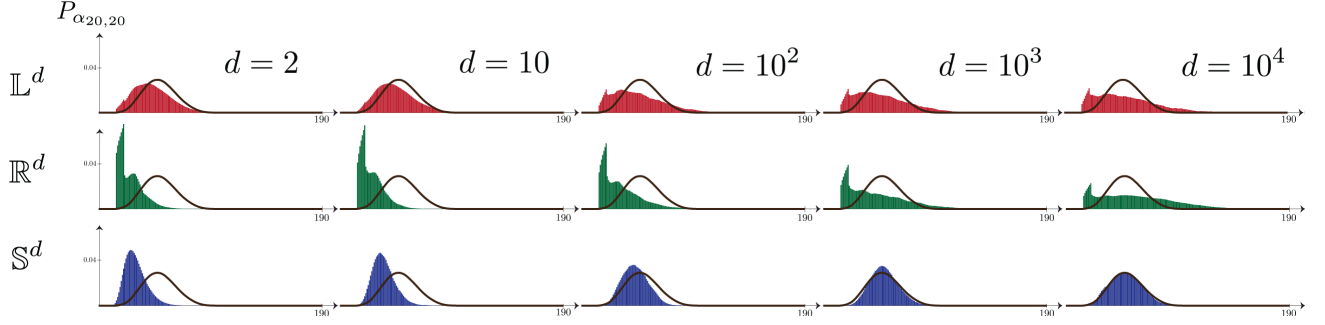


Figure 15: Brown curves represent the empirical PMF of $\alpha_{20,20}$ from angle comparisons. In each row, we generate points from the corresponding space form of dimension d . This test detects a high-dimensional spherical space for the geometry of angle comparisons ($d^* = 10000$).

RFA index comparisons: This test identifies 1000-dimensional spherical space as the geometry of RFA index comparisons; see Figure 16.

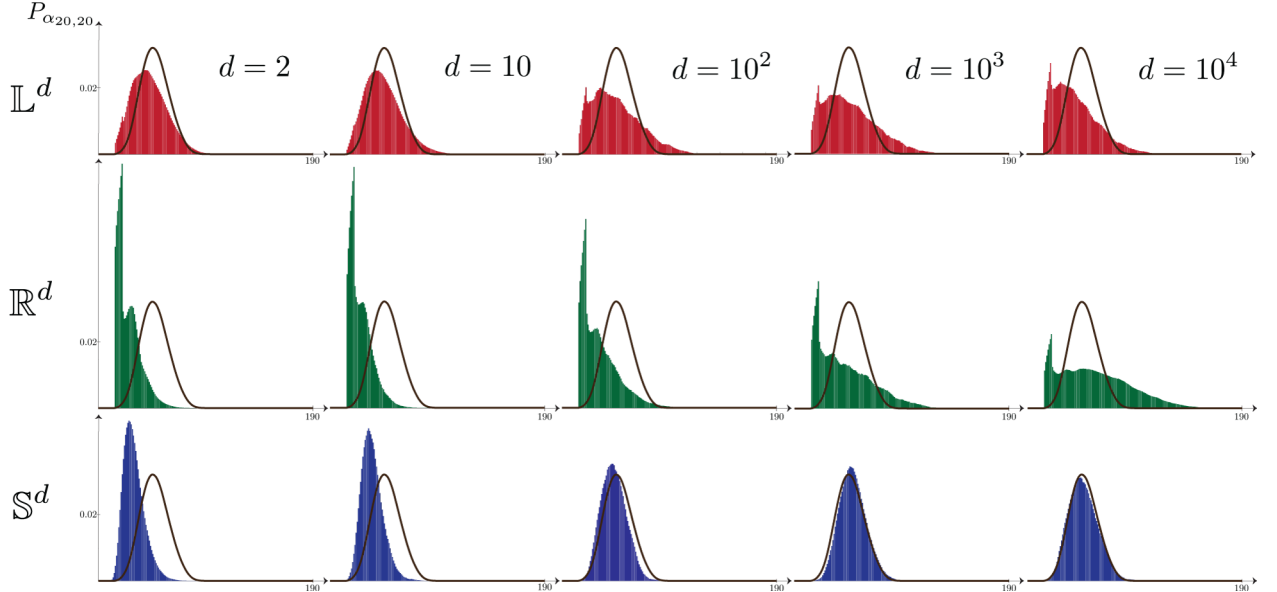


Figure 16: Brown curves represent the empirical PMF of $\alpha_{20,20}$ derived from RFA index comparisons. In each row, we generate points from the corresponding space form of dimension d . This test detects a high-dimensional spherical space ($d^* = 1000$) for the geometry of RFA index comparisons.

For embedding ordinal measurements, we pick a random clique of size 200 and embed it in low-dimensional space forms of different dimensions. Then, we compute the empirical probability of erroneous comparison, i.e., error occurs if $d(x_i, x_j) \geq d(x_k, x_l)$ whereas the points x_i, x_j are more similar to each other compared to the points x_k, x_l . We repeat the experiment 200 times, and report the mean and standard deviations of the probability of error p_e . In Section 9, we discuss the details of embedding algorithms used in this paper.

9 EMBEDDING ALGORITHMS

We can use semidefinite programs to solve non-metric embedding problems in hyperbolic and Euclidean spaces [33, 1]. The main objects in these problems are distance matrices, and the matrix of inner products, e.g., Gramian in Euclidean space and Lorentzian matrix in hyperbolic space. The traditional interior point method to solve

semidefinite programs do not scale to large problems. This is especially the case for non-metric embedding problems in which we have $\binom{N}{2} = O(N^2)$ distinct inequality constraints related to pairwise distance comparisons. Therefore, we propose non-metric embedding algorithms based on the method of alternative projections; see Algorithms 1 to 3.

9.1 Hyperbolic Embedding

We start with an arbitrary hyperbolic distance matrix (refer to [33]), and an index matrix; see **Example 1**. The function `IndexMatrix(D)` computes the index matrix associated with the distance matrix D .

We begin with sorting the elements of D according to the target index matrix Λ . In other words, we have

$$\text{sort}(D, \Lambda) = (d_{\pi(i,j)})_{i,j \in [N]}$$

where $\pi : [N]^2 \rightarrow [N]^2$ is a one-to-one map, such that $\pi(i,j) = \pi(j,i)$, $\pi(i,i) = (i,i)$, and $\text{IndexMatrix}(\text{sort}(D, \Lambda)) = \Lambda$. The resulting symmetric matrix is no longer a valid hyperbolic distance matrix. Therefore, we proceed with finding the best rank- $(d+1)$ Lorentzian matrix—the matrix of Lorentzian inner products. We compute the corresponding point set, in \mathbb{R}^{d+1} , by a simple spectral factorization of the Lorentzian matrix; see Algorithm 1 lines 6–8 and refer to [33]. Finally, we use a simple method to map each point (columns of X) to \mathbb{L}^d , viz.,

$$P_{\mathbb{R}^{d+1} \rightarrow \mathbb{L}^d}(x) = \begin{bmatrix} \sqrt{1 + \|y\|^2} \\ y \end{bmatrix} \text{ where } y = (x_2, \dots, x_{d+1})^\top.$$

We compute the hyperbolic Gramian, $G = X^\top H X$, where $H = \text{diag}(-1, 1, \dots, 1) \in \mathbb{R}^{(d+1) \times (d+1)}$. This gives us the update for hyperbolic distance matrix $D = \text{acosh}[-G]$; refer to [33]. We repeat this process till convergence.

Algorithm 1 Non-metric hyperbolic embedding

```

1: procedure HYPERBOLICEMBEDDING( $\Lambda, d$ )
2:   input: Index matrix  $\Lambda$ , and embedding dimension  $d$ .
3:   initialize: hyperbolic distance matrix  $D$ , and an arbitrary index matrix  $\tilde{\Lambda}$ .
4:   while  $\|\tilde{\Lambda} - \text{IndexMatrix}(D)\| > 0$  do
5:      $\tilde{\Lambda} \leftarrow \text{IndexMatrix}(D)$ . ▷ The index matrix related to  $D$ .
6:      $D \leftarrow \text{sort}(D, \Lambda)$ . ▷ Update  $D$  by sort distances according to  $\Lambda$ .
7:     Let  $U \Sigma U^\top$  be the eigenvalue decomposition of  $G = -\cosh[D]$  such that  $\sigma_1 \geq \dots \geq \sigma_N \in \mathbb{R}$ .
8:      $X = |\Sigma_d|^{1/2} U_d^\top$ , where  $\Sigma_d = \text{diag}[(\sigma_1)_+, \dots, (\sigma_d)_+, (\sigma_N)_-]$  and  $U_d$  is the sliced eigenvector matrix.
9:      $X \leftarrow P_{\mathbb{R}^{d+1} \rightarrow \mathbb{L}^d}(X)$ . ▷ Map each column of  $X \in \mathbb{R}^{(d+1) \times N}$  to  $\mathbb{L}^d$ .
10:     $G = X^\top H X$ . ▷ Hyperbolic Gramian.
11:     $D \leftarrow \text{acosh}[-G]$ . ▷ Hyperbolic distance matrix.
12:   end while
13:   return  $X$ 
14: end procedure

```

9.2 Spherical Embedding

We propose a similar method for spherical embedding. The matrix of inner products G and the spherical distance matrix D are related via $D = \text{acos}[G]$. For points in d -dimensional spherical space, the matrix G is a positive semidefinite matrix of rank $(d+1)$, and with diagonal elements of 1. The spectral factorization of G gives us the point positions.

At each iteration of Algorithm 2, we shuffle the elements of the distance matrix according to the target index matrix, but the corresponding Gram matrix $G = \cos[\text{sort}(D, \Lambda)]$ is not a valid Gram matrix for points in \mathbb{S}^d . We first find the best rank- $(d+1)$ positive semidefinite matrix via a simple eigenvalue thresholding which gives a set of points in \mathbb{R}^{d+1} —as opposed to \mathbb{S}^d ; see line 9 of Algorithm 2. Therefore, we radially project each point to \mathbb{S}^d , i.e., $P_{\mathbb{R}^{d+1} \rightarrow \mathbb{S}^d}(x) = \frac{1}{\|x\|}x$. We repeat this process till a convergence is achieved.

Algorithm 2 Non-metric spherical Embedding

```

1: procedure SPHERICALEMBEDDING( $\Lambda$ )
2:   input: Index matrix  $\Lambda$ , and embedding dimension  $d$ .
3:   initialize: Spherical distance matrix  $D$ , and an arbitrary index matrix  $\tilde{\Lambda}$ .
4:   while  $\|\tilde{\Lambda} - \text{IndexMatrix}(D)\| > 0$  do
5:      $\tilde{\Lambda} \leftarrow \text{IndexMatrix}(D)$ . ▷ The index matrix related to  $D$ .
6:      $D \leftarrow \text{sort}(D, \Lambda)$ . ▷ Update  $D$  by sort distances according to  $\Lambda$ .
7:     Let  $U\Sigma U^\top$  be eigenvalue decomposition of  $G = \cos[D]$  such that  $\sigma_1 \geq \dots \geq \sigma_N \in \mathbb{R}$ .
8:     Let  $\Sigma_d = \text{diag}[(\sigma_1)_+, \dots, (\sigma_{d+1})_+]$ , and  $U_d$  be corresponding eigenvector matrix.
9:      $X = \Sigma_d^{1/2} U_d^\top$ .
10:     $X \leftarrow P_{\mathbb{R}^{d+1} \rightarrow \mathbb{S}^d}(X)$ . ▷ Map each column of  $X \in \mathbb{R}^{(d+1) \times N}$  to  $\mathbb{S}^d$ .
11:     $G = X^\top X$ . ▷ The Gram matrix.
12:     $D \leftarrow \text{acos}[G]$ .
13:   end while
14:   return  $X$ 
15: end procedure

```

9.3 Euclidean Embedding

Unlike hyperbolic and spherical counterparts, Euclidean distance matrix $D \in \mathbb{R}^{N \times N}$ is the matrix of squared distances between a set of N points $X \in \mathbb{R}^{d \times N}$. This definition lets us to express it as a linear function of the Gram matrix $G = X^\top X$, i.e., $D = \mathcal{K}(G) = -2G + \text{diag}(G)1^\top + 1\text{diag}(G)^\top$, where $\text{diag}(G)$ is a vector of diagonal elements of G , and $1 \in \mathbb{R}^N$ is the vector of all ones. The Gram matrix G is positive semidefinite of rank at most d . We can find the centered Gramian from a given distance matrix as $G = -\frac{1}{2}JDJ$, where $J = I - \frac{1}{N}11^\top$. At each iteration of Algorithm 3, we find the best rank- d positive semidefinite matrix via a simple eigenvalue thresholding of $G = -\frac{1}{2}JDJ$; see lines 7 – 8 of Algorithm 3. The spectral factorization of G gives the point set in \mathbb{R}^d . We repeat this process until convergence.

Algorithm 3 Non-metric Euclidean embedding

```

1: procedure EUCLIDEANEMBEDDING( $\Lambda$ )
2:   input: Index matrix  $\Lambda$ , and embedding dimension  $d$ .
3:   initialize: hyperbolic distance matrix  $D$ , and an arbitrary index matrix  $\tilde{\Lambda}$ .
4:   while  $\|\tilde{\Lambda} - \text{IndexMatrix}(D)\| > 0$  do
5:      $\tilde{\Lambda} \leftarrow \text{IndexMatrix}(D)$ . ▷ The index matrix related to  $D$ .
6:      $D = \text{sort}(D, \Lambda)$ .
7:     Let  $U\Sigma U^\top$  be the eigenvalue decomposition of  $G = -\frac{1}{2}JDJ$  such that  $\sigma_1 \geq \dots \geq \sigma_N \in \mathbb{R}$ .
8:      $G = U_d \Sigma_d U_d^\top$ , where  $\Sigma_d = \text{diag}[(\sigma_1)_+, \dots, (\sigma_d)_+]$  and  $U_d$  is the sliced eigenvector matrix.
9:      $D \leftarrow \mathcal{K}(G)$ . ▷ Euclidean distance matrix.
10:   end while
11:   return  $X = \Sigma_d^{1/2} U_d^\top$ .
12: end procedure

```

References

- [1] Sameer Agarwal, Josh Wills, Lawrence Cayton, Gert Lanckriet, David Kriegman, and Serge Belongie. Generalized non-metric multidimensional scaling. In *Artificial Intelligence and Statistics*, pages 11–18, 2007.
- [2] Michael Ashburner, Catherine A Ball, Judith A Blake, David Botstein, Heather Butler, J Michael Cherry, Allan P Davis, Kara Dolinski, Selina S Dwight, Janan T Eppig, et al. Gene ontology: tool for the unification of biology. *Nature genetics*, 25(1):25–29, 2000.
- [3] Shuanghua Bai, Huo-Duo Qi, and Naihua Xiu. Constrained best euclidean distance embedding on a sphere: a matrix optimization approach. *SIAM Journal on Optimization*, 25(1):439–467, 2015.
- [4] Gunnar Carlsson. Topology and data. *Bulletin of the American Mathematical Society*, 46(2):255–308, 2009.

- [5] P CHEBOTAREV and EV SHAMIS. The matrix-forest theorem and measuring relations in small social groups. *Automation and remote control*, 58(9):1505–1514, 1997.
- [6] Thomas H Cormen, Charles E Leiserson, Ronald L Rivest, and Clifford Stein. *Introduction to algorithms*. MIT press, 2009.
- [7] Gordon M Crippen, Timothy F Havel, et al. *Distance geometry and molecular conformation*, volume 74. Research Studies Press Taunton, 1988.
- [8] Zhenghang Cui, Nontawat Charoenphakdee, Issei Sato, and Masashi Sugiyama. Classification from triplet comparison data. *Neural Computation*, 32(3):659–681, 2020.
- [9] Çağatay Demiralp, Michael S Bernstein, and Jeffrey Heer. Learning perceptual kernels for visualization design. *IEEE transactions on visualization and computer graphics*, 20(12):1933–1942, 2014.
- [10] Ivan Dokmanic, Reza Parhizkar, Juri Ranieri, and Martin Vetterli. Euclidean distance matrices: Essential theory, algorithms, and applications. *IEEE Signal Processing Magazine*, 32(6):12–30, 2015.
- [11] Asi Elad, Yosi Keller, and Ron Kimmel. Texture mapping via spherical multi-dimensional scaling. In *International Conference on Scale-Space Theories in Computer Vision*, pages 443–455. Springer, 2005.
- [12] Chad Giusti, Eva Pastalkova, Carina Curto, and Vladimir Itskov. Clique topology reveals intrinsic geometric structure in neural correlations. *Proceedings of the National Academy of Sciences*, 112(44):13455–13460, 2015.
- [13] Robin M Green and Robin Michael Green. *Spherical astronomy*. Cambridge University Press, 1985.
- [14] Siavash Haghir, Debarghya Ghoshdastidar, and Ulrike von Luxburg. Comparison-based nearest neighbor search. In *Artificial Intelligence and Statistics*, pages 851–859, 2017.
- [15] Siavash Haghir, Damien Garreau, and Ulrike Luxburg. Comparison-based random forests. In *International Conference on Machine Learning*, pages 1871–1880, 2018.
- [16] Wassily Hoeffding. A class of statistics with asymptotically normal distribution. In *Breakthroughs in statistics*, pages 308–334. Springer, 1992.
- [17] Shuai Huang and Ivan Dokmanić. Reconstructing point sets from distance distributions. *arXiv preprint arXiv:1804.02465*, 2018.
- [18] Kevin G Jamieson and Robert Nowak. Active ranking using pairwise comparisons. In *Advances in Neural Information Processing Systems*, pages 2240–2248, 2011.
- [19] Kevin G Jamieson and Robert D Nowak. Low-dimensional embedding using adaptively selected ordinal data. In *2011 49th Annual Allerton Conference on Communication, Control, and Computing (Allerton)*, pages 1077–1084. IEEE, 2011.
- [20] Matthäus Kleindessner and Ulrike Luxburg. Uniqueness of ordinal embedding. In *Conference on Learning Theory*, pages 40–67, 2014.
- [21] Anna Klimovskaia, David Lopez-Paz, Léon Bottou, and Maximilian Nickel. Poincaré maps for analyzing complex hierarchies in single-cell data. *Nature Communications*, 11(1):1–9, 2020.
- [22] Joseph B Kruskal. Nonmetric multidimensional scaling: a numerical method. *Psychometrika*, 29(2):115–129, 1964.
- [23] Matt Le, Stephen Roller, Laetitia Papaxanthos, Douwe Kiela, and Maximilian Nickel. Inferring concept hierarchies from text corpora via hyperbolic embeddings. *arXiv preprint arXiv:1902.00913*, 2019.
- [24] John M Lee. *Riemannian Manifolds: An Introduction to Curvature*. Springer New York, 2007.
- [25] Leo Liberti, Carlile Lavor, Nelson Maculan, and Antonio Mucherino. Euclidean distance geometry and applications. *SIAM review*, 56(1):3–69, 2014.
- [26] Daniel J Navarro and Michael D Lee. Common and distinctive features in stimulus similarity: A modified version of the contrast model. *Psychonomic Bulletin & Review*, 11(6):961–974, 2004.
- [27] Mireya Plass, Jordi Solana, F Alexander Wolf, Salah Ayoub, Aristotelis Misios, Petar Glažar, Benedikt Obermayer, Fabian J Theis, Christine Kocks, and Nikolaus Rajewsky. Cell type atlas and lineage tree of a whole complex animal by single-cell transcriptomics. *Science*, 360(6391), 2018.
- [28] Josep M Porta, Lluís Ros, Federico Thomas, and Carme Torras. A branch-and-prune solver for distance constraints. *IEEE Transactions on Robotics*, 21(2):176–187, 2005.

- [29] Robert Alexander Rankin. The closest packing of spherical caps in n dimensions. *Glasgow Mathematical Journal*, 2(3):139–144, 1955.
- [30] Roger N Shepard. The analysis of proximities: multidimensional scaling with an unknown distance function. i. *Psychometrika*, 27(2):125–140, 1962.
- [31] Roger N Shepard. The analysis of proximities: Multidimensional scaling with an unknown distance function. ii. *Psychometrika*, 27(3):219–246, 1962.
- [32] Anthony Man-Cho So and Yinyu Ye. Theory of semidefinite programming for sensor network localization. *Mathematical Programming*, 109(2-3):367–384, 2007.
- [33] Puoya Tabaghi and Ivan Dokmanić. Hyperbolic distance matrices. In *Proceedings of the 26th ACM SIGKDD International Conference on Knowledge Discovery & Data Mining*, page 1728–1738, 2020.
- [34] Puoya Tabaghi, Ivan Dokmanić, and Martin Vetterli. Kinetic Euclidean distance matrices. *IEEE Transactions on Signal Processing*, 68:452–465, 2019.
- [35] Omer Tamuz, Ce Liu, Serge Belongie, Ohad Shamir, and Adam Tauman Kalai. Adaptively learning the crowd kernel. *arXiv preprint arXiv:1105.1033*, 2011.
- [36] Amos Tanay and Aviv Regev. Scaling single-cell genomics from phenomenology to mechanism. *Nature*, 541(7637):331–338, 2017.
- [37] Pál Turán. On an external problem in graph theory. *Mat. Fiz. Lapok*, 48:436–452, 1941.
- [38] Laurens Van Der Maaten and Kilian Weinberger. Stochastic triplet embedding. In *2012 IEEE International Workshop on Machine Learning for Signal Processing*, pages 1–6. IEEE, 2012.
- [39] Kevin Verbeek and Subhash Suri. Metric embedding, hyperbolic space, and social networks. In *Proceedings of the thirtieth annual symposium on Computational geometry*, pages 501–510, 2014.
- [40] Fabian Wauthier, Michael Jordan, and Nebojsa Jojic. Efficient ranking from pairwise comparisons. In *International Conference on Machine Learning*, pages 109–117, 2013.
- [41] Richard C Wilson, Edwin R Hancock, Elżbieta Pełkalska, and Robert PW Duin. Spherical embeddings for non-Euclidean dissimilarities. In *2010 IEEE Computer Society Conference on Computer Vision and Pattern Recognition*, pages 1903–1910. IEEE, 2010.
- [42] Aaron D Wyner. Random packings and coverings of the unit n -sphere. *The Bell System Technical Journal*, 46(9):2111–2118, 1967.
- [43] Yuansheng Zhou, Brian H Smith, and Tatyana O Sharpee. Hyperbolic geometry of the olfactory space. *Science advances*, 4(8):eaq1458, 2018.